Integral formulation and simulations of falling and sheared thin films

Amélie Simon, Jean-Marc Hérard, Meryem Marcelet

Integral formulation and simulations of falling and sheared thin films

Amélie Simon[1,3], Jean-Marc Hérard[1,2], Meryem Marcelet[1]

[1] EDF R&D - MFEE - 6 quai watier, 78400, Chatou, France
[2] I2M - UMR CNRS 7373 - F13453 Marseille, France
[3] LMFA - UMR CNRS 5509 - Ecole Centrale de Lyon, 69134, Ecully, France

19 septembre 2017

Abstract

In the electricity production, studying liquid films in steam turbines contributes to reduce damages and losses due to wetness. Thin liquid films are created by the deposition of droplets and are highly sheared by surrounding steam. Up to now, no comprehensive and validated model has arisen to describe this phenomenon. Thus, a 2D model based on an integral formulation associated with closure laws is developed to represent this film. Compared to classical Shallow-Water equation, the model takes into account additional effects such as mass transfer, droplet impact, shearing at the free surface, surface tension, pressure gradient and rotation effects. The model properties (hyperbolicity, entropy inequality, linear stability, Galilean and rotational invariance) are examined in order to evaluate the relevance of the model. A 2D code is implemented in the EDF code Code_Saturne which relies on finite volume method for unstructured meshes. The model, which degenerates into classical Shallow-Water equations for the case of a falling liquid film on a inclined plane, is validated using the experiment of [Liu and Gollub, 1994] and is compared to reference models ([Ruyer-Quil and Manneville, 2000] and [Lavalle, 2014]). Sheared film under low-pressure steam turbine conditions are simulated and also validated using the experiment of [Hammitt et al., 1981]. Unsteady simulations show that the surface tension effects are of great importance; they also give the main features in the behavior of liquid film under realistic low-pressure steam turbine conditions.

1 INTRODUCTION

Steam turbines produce over 80 % of the world's electricity. The improvement of the efficiency of turbines would lead to a considerable gain in natural resources. In the electricity production chain, the steam turbine converts steam thermal energy into mechanical energy of rotation. Steam turbine is composed of a succession of stages, each stage being composed of a row of fixed blades (stators) and a row of moving blades (rotors). The steam flows through the turbine at high speed, between 80 and 400 m/s. During the fast expansion of originally dry steam, wetness appears. A fog of small droplets with diameter from 0.1 to 2 μm is suddenly created mostly by homogeneous nucleation. Unlike heterogeneous nucleation, this process does not involve nucleation sites. These droplets grow either by condensation of the steam or by coalescence. A part of these droplets is deposited on solid surfaces such as blades. The accumulation of this deposition produces a thin layer of water, also called liquid film. Drops are then removed from this liquid film by atomization at the free surface or at the geometrical edge. Back in the steam flow, these drops break up into smaller drops. These drops remains at least one order of magnitude bigger than nucleated droplets. Then, a part of this atomized drops impacts the following rows of blades. The cascade of wet phenomena in steam turbines results in five distinct stages, namely nucleation, growth, deposition, liquid film and atomization.

Unfortunately, wetness has negative consequences in steam turbine. The impact of atomized drops with a diameter superior to 50 μm leads to erosion ([Moore and Sieverding, 1976]). The liquid film running down the turbine shaft can induce vibration crisis ([Stanciu et al.,]). And, all the phenomena related to wetness induce losses which represents 25 % of total turbine losses. This efficiency issue motivated the study of liquid films. An order of magnitude of these losses is given by the Baumann rule in 1912 which predicts 1 % of turbine power loss for 1 % humidity ([Baumann, 1912]). More recently, classifications of the various wetness losses in steam

turbines has been specified by [Gyarmathy, 1962], [Laali, 1991], [White, 1992] or [Fendler, 2012]. For each wet phenomenon is associated a particular wetness loss. Since the liquid film can contribute largely to the total wet losses (directly and indirectly because of generated large drops that slow down the steam flow), this paper concentrates on related losses. Direct losses come from the friction of the liquid film with the steam and the presence of the film which adds resistance to shaft's rotation. In order to estimate losses due to friction, the thickness of the liquid film and the frequency of the waves at the free surface of the liquid film are needed, and to calculate losses due to inertial resistance to rotation, the position of the film on the rotor and the flow rate of the liquid film are required. Then, the general objective is to obtain numerically these data to estimate precisely the loss induced by the liquid film.

Before presenting the state of the art of liquid film models in steam turbines, let's return to the description of the real phenomenon. Figure 1 summarizes all the effect affecting the liquid film. Regarding the mass balance, the liquid film is created by the deposition of the droplets coming from the nucleation as well as the deposition of the atomized drops of the previous row of blades. Drops are also atomized from the liquid film at the free surface and at the geometric edges. Heat transfer (condensation/evaporation) affects the mass balance of the liquid film but to a lesser extent in pure operating conditions. The film is subjected to gravity, steam pressure, steam shear at the free surface, friction on the wall, droplet impact, surface tension, and to rotation for the rotor case.

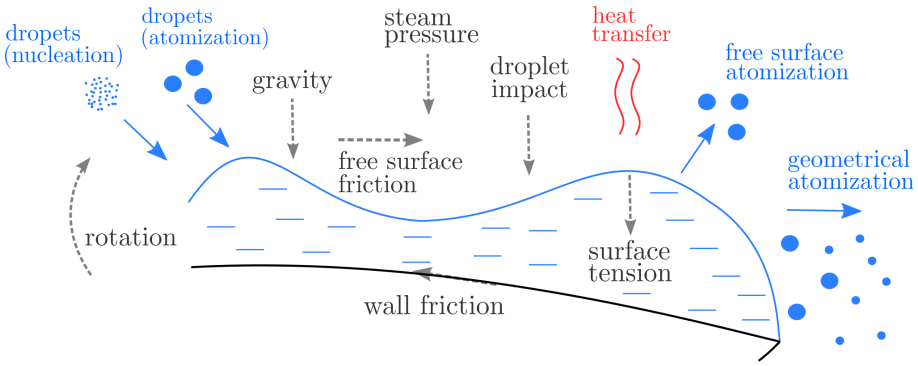

Figure 1: Real phenomena around a liquid film on a steam turbine blade

The magnitude of the height of the liquid film according to [Moore and Sieverding, 1976] is 10 μm and according to [Hammitt et al., 1981] is between 10 and 100 μm. The wavelength of the waves at the free surface is estimated between 0.1 to 100 mm ([Hammitt et al., 1981]). An rough estimate of the Reynolds numbers of the film suggests that the film is laminar. These characteristics will be useful for the choice of the model.

Liquid film in steam turbines is a complex phenomena which is seldomly discussed in the scientific community. The objective of this study is to describe the unsteady liquid film in steam turbine with a validated model and robust numerical simulations. Simulations in real configurations coupled with the steam phase is out of the scope of this paper but preliminary tests can be found in chapter 8 of [Simon, 2017] using the steam data obtained by [Blondel, 2014]. In the field of liquid films outside from turbines applications, new models are published, even recently, to accurately represent a liquid film falling on an inclined wall ([Ruyer-Quil and Manneville, 2000], [Lavalle, 2014], [Richard et al., 2016]). This simplified configuration with respect to the mechanisms present in a steam turbine is still under study. In the literature for liquid film in steam turbine, few models exist but none of them undertakes all the effects and are validated by experiments. In the case of stator models (without rotation), [Hammitt et al., 1981] assume that the shear of the free surface steam predominates, and using empirical correlations for the free surface friction, they constructed a stationary Couette model. [Gyarmathy, 1962] uses the same theoretical approach by adding the impact of the drops. [Kirillov and Yablonik, 1970] did not take into account the impact of the drops but added the pressure of the steam. [Malamatenios et al., 1994] significantly improve these models by taking into account convection, free surface shear and gravity with integral formulation. In the case of the rotor models (with rotation), a stationary approach is proposed by [Gyarmathy, 1962] taking only the centrifugal effects into account. An unsteady model is presented by [Kirillov and Yablonik, 1970] with convection, wall friction, centrifugal effects and Coriolis. [Williams and Young, 2007] improve it by adding shear

to the free surface and the gas pressure gradient, and also by giving explicitly the coefficient of friction at the wall. Using an integral formulation, [Schuster et al., 2014] add to the latter model the mass transfer and the impact of the drops for the study of liquid film on a radial turbine. Finally, the work of [Fendler, 2012], carried out within the EDF research center, is based on the [Foucart, 1999] integral formulation model, initiated for liquid films on walls of internal combustion engines. This model takes into account convection, mass transfer, wall friction and shear at the free surface. However, due to the simplifying assumptions adopted, and in particular due to the fact that surface tension is not taken into account, these models are not able to correctly reproduce wave generation at the free surface of liquid films and consequently can not describe precisely either the friction at the interface or the preparatory phases of the atomization. The model proposed in this paper is an instantaneous and relatively complete model for liquid films on stators and rotors in steam turbines. It takes into account more physical effects: for example, the additional surface tension effects and gravity with respect to the [Schuster et al., 2014] model, or surface tension, gravity, gas pressure and the impact of the drops with respect to the model of [Fendler, 2012]. On top of that, special attention is paid to analyze the properties of the model and to validate it.

2 THE LIQUID FILM MODEL

The establishment of the model which represents a liquid film on steam turbines is rigorously presented by specifying all the assumptions made. This model is an integrated formulation (Saint-Venant or Shallow-Water equations type) and solves the thickness and the velocity of the film. The model comes from the incompressible Navier–Stokes equations written in a rotating frame. These equations are simplified by neglecting the terms with respect to a chosen order. The simplified equations are integrated through the thickness of the film. To explicit the formulation, some terms need closure laws. Once chosen, the analysis of the properties of the model is carried out.

2.1 The governing equations

2.1.1 Effects taken account in the model

The real phenomena of a liquid film in steam turbine are detailed on figure 1. With a view to simplification, the proposed model does not take into account the curvature of the blade. However, it handles all the described force: the inertial rotating forces, the gas pressure, the friction at the wall, the friction at the free surface, the gravity, the surface tension and the droplet impact. Besides, a mass source term is integrated in order to add mass transfer at the free surface due to droplets deposition (nucleated droplets or atomized drops from the previous row of blades), the atomization (at the free surface or at a geometrical border) as well as the condensation and the evaporation of the film. Figure 2 displays the effects handled by the model and is to be compared with the real phenomena displayed on figure 1.

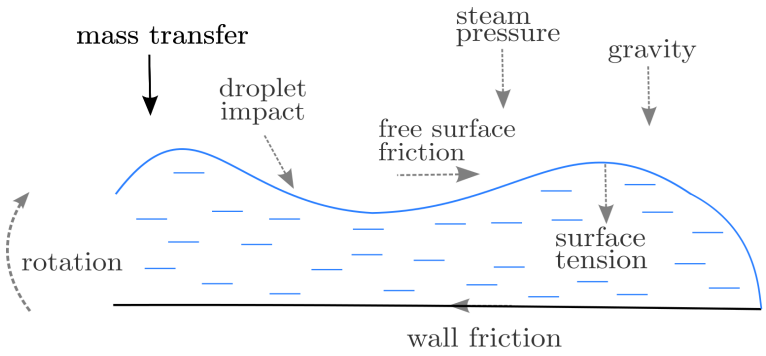

Figure 2: Effects handled by the model

A first hypothesis is adopted regarding droplets impact. When a droplet impacts the liquid film, on one side, it induces a variation on the mass and the momentum of the film, which will be taken into account by the

model. On the other side, it disturbs the free surface of the film. For this last consequence, we assume that the film relaxation of this perturbation is instantaneous, thus the free surface remains unchanged.

2.1.2 Geometrical configuration

The absolute reference frame $(\overrightarrow{x_0}, \overrightarrow{y_0}, \overrightarrow{z_0})$ is tied to the turbine shaft. The rotational vector $\overrightarrow{\Omega}$ is collinear to the axis $\overrightarrow{x_0}$ and its value ω_0 is constant. The system of equations is written in the local frame $(\overrightarrow{x}, \overrightarrow{y}, \overrightarrow{z})$ bound to the blade which is sketched as a flat plate as illustrated on figure 3. In this paper we consider the case where $\overrightarrow{x_0}$ depends on $\overrightarrow{x}$ only. In other words, this study is restricted to flat plates in the axis of the turbine shaft. The radius of the turbine shaft is r.

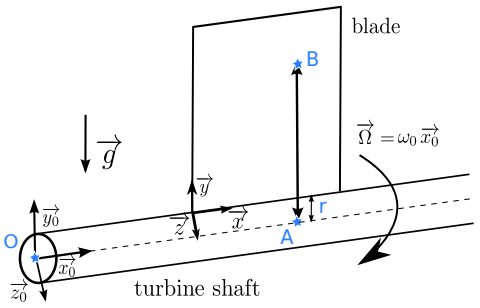

Figure 3: Absolute frame

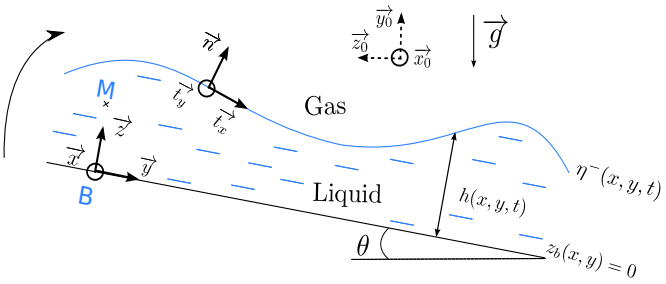

Figure 4: Local frame on the plate surface

The local frame associated to the free surface is $\left(\overrightarrow{t_x}, \overrightarrow{t_y}, \overrightarrow{n}\right)$ and is drawn on figure 4. The height of the film is h and the position of the free surface is η.

2.1.3 Boundary conditions

At the wall boundary, a classical no-slip boundary condition expression (1) is applied. We note, (u, v, w) the velocities components in the frame of reference $(\overrightarrow{x}, \overrightarrow{y}, \overrightarrow{z})$.

$$u_{|z_b} = v_{|z_b} = w_{|z_b} = 0 \tag{1}$$

Mass transfer (deposition, atomization, condensation and evaporation) is taken into account. To achieve this, a mass balance on an infinitesimal volume at the free surface (see figure 5) is done:

$$\frac{dm}{dt} = \rho \mathcal{S}_h dx dy \tag{2}$$

with $\mathcal{S}_h$ the mass transfer of the gas to the film in m/s.

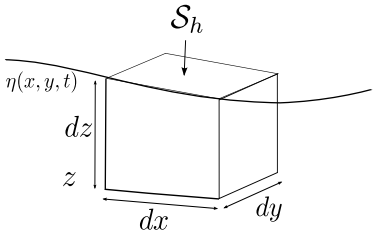

Figure 5: Infinitesimal volume at the free surface

If we assume a small curvature of the free surface, that is to say when $\eta(x, y) \simeq \eta(x + dx, y) \simeq \eta(x, y + dy)$ in figure 5, we find that, for an incompressible flow, the position of the free surface depends on the mass transfer as follows:

$$\frac{d\left(\eta - z\right)}{dt} = \mathcal{S}_h \tag{3}$$

The material derivative of $(\eta - z)$ represents the motion of a particle following the free surface. The equation (3) written in Euler variables is actually the kinematic boundary at the free surface:

$$w_{|\eta} = \frac{\partial \eta}{\partial t} + u_{|\eta}\frac{\partial \eta}{\partial x} + v_{|\eta}\frac{\partial \eta}{\partial y} - \mathcal{S}_h \tag{4}$$

Unlike in classical Shallow-Water equations, there is an additional mass transfer term in the kinematic boundary condition.

In paragraph 2.3 dealing with the closure laws, another boundary condition is needed. Therefore, the continuity of normal constraints at the free surface is assumed (see expression (16)).

2.1.4 Simplified Navier–Stokes equations

The incompressible Navier–Stokes equations (continuity and momentum) written in the local frame $(\overrightarrow{x}, \overrightarrow{y}, \overrightarrow{z})$ are read:

$$\begin{cases} \dfrac{\partial u}{\partial x} + \dfrac{\partial v}{\partial y} + \dfrac{\partial w}{\partial z} = 0 \\ \dfrac{\partial u}{\partial t} + \dfrac{\partial u^2}{\partial x} + \dfrac{\partial uv}{\partial y} + \dfrac{\partial uw}{\partial z} = -\dfrac{1}{\rho}\dfrac{\partial p}{\partial x} + \dfrac{1}{\rho}\dfrac{\partial \tau_{xx}}{\partial x} + \dfrac{1}{\rho}\dfrac{\partial \tau_{xy}}{\partial y} + \dfrac{1}{\rho}\dfrac{\partial \tau_{xz}}{\partial z} \\ \dfrac{\partial v}{\partial t} + \dfrac{\partial uv}{\partial x} + \dfrac{\partial v^2}{\partial y} + \dfrac{\partial vw}{\partial z} = g\sin\theta - \dfrac{1}{\rho}\dfrac{\partial p}{\partial y} + \dfrac{1}{\rho}\dfrac{\partial \tau_{xy}}{\partial x} + \dfrac{1}{\rho}\dfrac{\partial \tau_{yy}}{\partial y} + \dfrac{1}{\rho}\dfrac{\partial \tau_{yz}}{\partial z} + \omega_0^2(r+y) + 2\omega_0 w \\ \dfrac{\partial w}{\partial t} + \dfrac{\partial uw}{\partial x} + \dfrac{\partial vw}{\partial y} + \dfrac{\partial w^2}{\partial z} = -g\cos\theta - \dfrac{1}{\rho}\dfrac{\partial p}{\partial z} + \dfrac{1}{\rho}\dfrac{\partial \tau_{xz}}{\partial x} + \dfrac{1}{\rho}\dfrac{\partial \tau_{yz}}{\partial y} + \dfrac{1}{\rho}\dfrac{\partial \tau_{zz}}{\partial z} + \omega_0^2 z - 2\omega_0 v \end{cases} \tag{5}$$

with p the liquid pressure and τ the shear stress, both in $kg/(ms^2)$. As the rotational vector is in the x-direction, the rotation induces contributions in the y-direction and z-direction. No mass term has been added in the continuity equation (or droplets impact effect in the momentum equations) since within the liquid film volume there is no mass transfer. To compare the order of magnitude of all terms, a dimensional analysis is carried. In table 1, the stars * indicate the adopted non-dimensional variables, with λ, the characteristic wavelength of the free surface of the film, the subscript g referring to the gas and the subscript 0 as well as the capital letters denoting the characteristic variables.

$x = x^*\lambda$	$y = y^*\lambda$	$z = z^* h_0$
$(r+y) = (r+y)^*\lambda$	$\eta = \eta^* h_0$	$t = t^*\,(\lambda/u_0)$
$u = u^* u_0$	$v = v^* u_0$	$w = w^* w_0$
$p = p^*\rho u_0^2$	$g\sin\theta = g^* g_0$	$g\cos\theta = g^* g_0$
$u_g = u_g^* U_g$	$v_g = v_g^* U_g$	$w_g = w_g^* U_g$

Table 1: Non-dimensional variables

By introducing the non-dimensional variables in equations (5), four non-dimensional numbers naturally appear: the scale number $\varepsilon = h_0/\lambda$, the Reynolds number $Re = h_0 u_0/\nu$, the Froude number $Fr = u_0/\sqrt{g h_0}$ and the Rossby number $Ro = u_0/\omega_0\lambda$. To avoid a degenerated system, the three terms in the mass balance equation must be of the same order of magnitude, which leads to the relation $w_0 = u_0\varepsilon$.

It is assumed that $Re = \mathcal{O}(1)$, $Fr = \mathcal{O}(1)$ and $Ro = \mathcal{O}(1)$, thus only ε remains in system (5) with non-dimensional variables. The long wavelength assumption ($\lambda \to +\infty$) which is the most likely to occur in steam turbine as mentioned in introduction, implies that $\varepsilon \to 0$ and consequently that the most important terms are the ones with the smallest power of ε. We choose to keep the horizontal convection of the film and to neglect the vertical convection of the film. This decision comes down to neglecting terms equal or of order higher than $\mathcal{O}(\varepsilon^2)$. Besides, all the rotational terms are kept in order to obtain consistent properties of the model (see paragraph 2.5). Afterwards, the momentum equation in the z-direction is used to obtain the pressure. The latter pressure is then plugged into the momentum equation in the x-direction and y-direction. As the order

of magnitude of the pressure gradient term in the first two momentum equations is $\mathcal{O}(\varepsilon)$, it is consistent, to neglect terms of order $\mathcal{O}(\varepsilon)$ in the momentum equation in the z-direction. Hence, the Navier–Stokes equations up to order $\mathcal{O}(\varepsilon)$ read:

$$\begin{cases} \dfrac{\partial u}{\partial x}+\dfrac{\partial v}{\partial y}+\dfrac{\partial w}{\partial z}=0 \\ \dfrac{\partial u}{\partial t}+\dfrac{\partial u^2}{\partial x}+\dfrac{\partial uv}{\partial y}+\dfrac{\partial uw}{\partial z}=-\dfrac{1}{\rho}\dfrac{\partial p}{\partial x}+\dfrac{1}{\rho}\dfrac{\partial \tau_{xz-r}}{\partial z} \\ \dfrac{\partial v}{\partial t}+\dfrac{\partial uv}{\partial x}+\dfrac{\partial v^2}{\partial y}+\dfrac{\partial vw}{\partial z}=g\sin\theta-\dfrac{1}{\rho}\dfrac{\partial p}{\partial y}+\dfrac{1}{\rho}\dfrac{\partial \tau_{yz-r}}{\partial z}+\omega_0^2(r+y)+2\omega_0 w \\ \dfrac{\partial p}{\partial z}=-\rho g\cos\theta+\rho\omega_0^2 z-2\rho\omega_0 v \end{cases} \tag{6}$$

with the reduced shear stress terms at order $\mathcal{O}(\varepsilon)$: $\tau_{xz-r}=\mu\partial u/\partial z$ and $\tau_{yz-r}=\mu\partial v/\partial z$.

The expressions of the boundary conditions remain the same (equation (1) and equation (4)). When compared to classical Shallow-Water equations, the pressure field is not only hydrostatic but is also contains centrifugal and Coriolis contributions.

2.2 Film equations

To solve the average height and velocity at any position and time in the liquid film, the simplified Navier–Stokes equations (6) are integrated over the film thickness. Let us define the mean value of the height, h and of any quantity X as:

$$\begin{cases} h=\displaystyle\int_{z_b}^{\eta} dz \\ \overline{X}=\dfrac{1}{h}\displaystyle\int_{z_b}^{\eta} X dz \end{cases} \tag{7}$$

By applying the Leibniz rule and the boundary condition expressed equation (1), the continuity equation yields:

$$\frac{\partial}{\partial x}\int_{z_b}^{\eta} u dz-u_{|\eta}\frac{\partial \eta}{\partial x}+\frac{\partial}{\partial y}\int_{z_b}^{\eta} v dz-v_{|\eta}\frac{\partial \eta}{\partial y}+w_{|\eta}=0 \tag{8}$$

Thus, using the kinematic boundary condition (equation (4)) and the average definition (equation (7)) this result in:

$$\frac{\partial h}{\partial t}+\frac{\partial h\overline{u}}{\partial x}+\frac{\partial h\overline{v}}{\partial y}=\mathcal{S}_h \tag{9}$$

Furthermore, by integrating the z-momentum equation across the film thickness, we obtain the pressure field within the film which is:

$$p(x,y,z,t)=\mathscr{P}_{|\eta}+\rho g_z\left(z-\left(h(x,y,t)+z_b(x,y)\right)\right)+\frac{\rho\omega_0^2}{2}\left(z^2-\left(h(x,y,t)+z_b(x,y)\right)^2\right)+2\rho\omega_0\int_z^{\eta} v dz \tag{10}$$

where $\mathscr{P}_{|\eta}=p(x,y,\eta^-,t)$.

Proceeding the same way as for the continuity equation for the left hand side term and replacing the pressure with the integrated z-momentum equation, the x-momentum equation can be expressed as:

$$\begin{aligned} \frac{\partial h\overline{u}}{\partial t}+\frac{\partial}{\partial x}\int_{z_b}^{\eta} u^2 dz+\frac{\partial}{\partial y}\int_{z_b}^{\eta} uv dz=&-\frac{h}{\rho}\frac{\partial \mathscr{P}_{|\eta}}{\partial x}-hg\cos\theta\frac{\partial \eta}{\partial x}+\frac{\omega_0^2}{2}h\frac{\partial \eta^2}{\partial x} \\ &-2\omega_0\int_{z_b}^{\eta}\frac{\partial\int_z^{\eta} v dz}{\partial x}dz+\frac{1}{\rho}\left(\tau_{xz-r|\eta}-\tau_{xz-r|z_b}\right)+u_{|\eta}\mathcal{S}_h \end{aligned} \tag{11}$$

A remark is to be made concerning the droplet impact represented by the term $u_{|\eta}\mathcal{S}_h$. This one does not need to be added to equation (6) since it appears naturally during the integration step as long as there is a mass

transfer in the kinematic boundary condition at the free surface (4).

There is no additional difficulty to express the y-momentum equation. Eventually, the exact expression for the film model is:

$$\begin{cases} \dfrac{\partial h}{\partial t} + \dfrac{\partial h\overline{u}}{\partial x} + \dfrac{\partial h\overline{v}}{\partial y} = \mathcal{S}_h \\ \\ \dfrac{\partial h\overline{u}}{\partial t} + \dfrac{\partial}{\partial x}\left(\displaystyle\int_{z_b}^{\eta} u^2 dz + \frac{g\cos\theta h^2}{2}\right) + \frac{\partial}{\partial y}\int_{z_b}^{\eta} uv dz - \frac{\omega_0^2}{2} h\frac{\partial \eta^2}{\partial x} + 2\omega_0 \int_{z_b}^{\eta} \frac{\partial \int_z^{\eta} v dz}{\partial x} dz = \\ -\dfrac{h}{\rho}\dfrac{\partial \mathscr{P}_{|\eta}}{\partial x} - hg\cos\theta\dfrac{\partial z_b}{\partial x} + \dfrac{1}{\rho}\left(\tau_{xz-r|\eta} - \tau_{xz-r|z_b}\right) + u_{|\eta}\mathcal{S}_h \\ \\ \dfrac{\partial h\overline{v}}{\partial t} + \dfrac{\partial}{\partial x}\displaystyle\int_{z_b}^{\eta} uv dz + \frac{\partial}{\partial y}\left(\int_{z_b}^{\eta} v^2 dz + \frac{g\cos\theta h^2}{2}\right) - \frac{\omega_0^2}{2} h\frac{\partial \eta^2}{\partial y} + 2\omega_0 \int_{z_b}^{\eta} \frac{\partial \int_z^{\eta} v dz}{\partial y} dz - 2\omega_0 h\overline{w} = \\ g\sin\theta h - \dfrac{h}{\rho}\dfrac{\partial \mathscr{P}_{|\eta}}{\partial y} - hg\cos\theta\dfrac{\partial z_b}{\partial y} + \dfrac{1}{\rho}\left(\tau_{yz-r|\eta} - \tau_{yz-r|z_b}\right) + h\omega_0^2(r+y) + v_{|\eta}\mathcal{S}_h \end{cases} \tag{12}$$

The unknown solved by this model is the height of the film h, and the mean velocity components $\overline{u}$ and $\overline{v}$.

2.3 Closure laws

In order to close the model (12), the eight color terms need closure laws.

- To determine the pressure at the free surface of the film $\mathscr{P}_{|\eta}$, the surface tension is expressed using Laplace law. Indeed, for a thin films ($10\mu m$ to $100\mu m$ [Hammitt et al., 1981]), surface tension could play an important role. It may be written as:

$$\mathscr{P}_{|\eta^-} = \mathscr{P}_g + \frac{\sigma}{\mathscr{R}} \tag{13}$$

  where σ is the surface tension coefficient in kg/s^2 and $1/\mathscr{R}$ refers to the curvature of the free surface. The full expression can be found in [Wehausen and Laitone, 1960]. In this expression the higher order term of the surface tension appears at order $\mathcal{O}\left(\varepsilon^2\right)$ in the global model. Thus, the surface tension should be neglected, the simplified model (6) being at order $\mathcal{O}\left(\varepsilon\right)$. However, [Ruyer-Quil and Manneville, 1998] conclude that for falling film, surface tension contributes to the evolution of the pressure at the free surface and thus must be taken into account. Therefore, the expression of the curvature, which contains surface tension at order $\mathcal{O}\left(\varepsilon\right)$ in the global model is kept: $1/\mathscr{R} = -\left(\partial_{xx}\eta^- + \partial_{yy}\eta^-\right)$. The value $\mathscr{P}_g$, e.g. the pressure of the gas in the turbine, is prescribed using external aero-thermodynamic calculations of the expansion of the steam ([Fendler, 2012],[Blondel, 2014]).

- Turning to the wall stress $\overrightarrow{\tau_w} = (\tau_{xz-r|z_b}, \tau_{yz-r|z_b})^T$, we refer to the experimental work of [Spedding and Hand, 1997] for smooth and wavy free surface:

$$\underline{\tau}_w = \frac{c_{f,w}\rho|\overline{u}|\underline{\overline{u}}}{2} \tag{14}$$

  with the friction coefficient at the wall $c_{f,w} = 24/Re$ and with $\overline{u} = 1/h\int_0^h \underline{u}\left(z\right) dz$.
  When studying film without shear stress at the free surface (see section 4.1 on falling film), the wall friction is expressed in another classical way: assuming a parabolic velocity profile. This leads to:

$$\underline{\tau}_w = \frac{3\mu}{h}\underline{\overline{u}} \tag{15}$$

- Now, in order to obtain the shear at the free surface $\underline{\tau}_{int} = (\tau_{xz-r|\eta}, \tau_{yz-r|\eta})^T$, we use the continuity relation at the free surface:

$$\underline{\underline{\Sigma}}.\underline{n}_{|\eta^-} = \underline{\underline{\Sigma}}.\underline{n}^g_{|\eta^+} \tag{16}$$

where the normal vector n points outside of the liquid domain. The projection on the local frame $\left(\underline{t_x}, \underline{t_y}\right)$ (parallel to the free surface) assuming that $(\mu_g U_g)/(\mu u_0) = \mathcal{O}(1)$ and neglecting terms at order $\mathcal{O}\left(\varepsilon^2\right)$ is made in order to ensure consistency. We assume that :

$$\underline{\tau}_{int} = \frac{c_{f,int}\rho_g|\underline{u}_g - \underline{\overline{u}}|(\underline{u}_g - \underline{\overline{u}})}{2} \tag{17}$$

with $c_{f,int}$, the friction coefficient at the free surface prescribed by [Ihnatowicz et al., 1979] for liquid film in steam turbine:

$$c_{f,int} = \left(0.0007 + 0.0625 Re_g^{-0.32}\right)(1 + 0.025 Re) \tag{18}$$

- Special attention is paid to the velocity $u_{|_\eta}$ and $v_{|_\eta}$ arising with the mass transfer. In order to better understand these terms, a energy equation of a global system is derived, composed with droplets and gas using a statistic two-fluid model (see appendix A). It is first assumed that the velocity of the free surface depends on the velocity of the two phases and also that the mass transfer between the two phases is only due to thermodynamic phenomena; by enforcing a decrease of the energy with respect to time, this yields:

$$\begin{cases} u_{|\eta} = \dfrac{\overline{u} + u_g}{2} \\ v_{|\eta} = \dfrac{\overline{v} + v_g}{2} \end{cases} \tag{19}$$

  This closure law equation (19) differs fundamentally from previous work regarding droplet impact ([Stanton and Rutland, 1998], [Schuster et al., 2014] and [Delestre, 2010]) which do not consider a dependency of the film itself.

- In a first attempt to explicit the term $\mathcal{S}_h$, we assume that the liquid film is only fed by nucleated droplets, and once deposited these droplets fully stick to the film ([Moore and Sculpher, 1969], [Stanton and Rutland, 1998], [Schuster et al., 2014]). We then use the local concentration of droplets and the local gas velocity within a wet steam flow around a steam turbine computed by [Blondel, 2014] and traduce the deposition rate using the Zaichik correlation ([Zaichik et al., 1995] or [Zaichik et al., 2010]). This formulation gives a deposition rate J^+, in m/s, depending on the droplet volume concentration c_v, the wall friction velocity u^* and the deposition coefficient j^+, such as:

$$J^+ = j^+ \times c_v \times u^* \tag{20}$$

  where the deposition coefficient j^+ is:

$$j^+ = \frac{0.115 \times Sc^{-0.75} + 2.5 \times 10^{-4}\left(\tau^+\right)^{2.5}}{1 + 10^{-3} \times \left(\tau^+\right)^{2.5}} \tag{21}$$

  and where the Schmidt number is based on the Brownian coefficient such as $Sc = \nu_g / c_{dif}$. This Brownian coefficient reads :

$$c_{dif} = \frac{\mathcal{R} \times T_g}{6\pi \mathcal{N} \nu_g \rho_g} \tag{22}$$

  with the ideal gas constant and the Avogadro number respectively $\mathcal{R} = 8.31446\ J/(molK)$ and $\mathcal{N} = 6,022 \times 10^{23}\ mol^{-1}$.

- The non-linear terms $\int_{z_b}^{\eta} u^2 dz$, $\int_{z_b}^{\eta} uv dz$ and $\int_{z_b}^{\eta} v^2 dz$, can be exactly calculated by enforcing a velocity profile to the film. We introduce the profile factor Γ, a constant value depending on the velocity profile only, such that:

$$\begin{cases} \displaystyle\int_{z_b}^{\eta} u^2 dz = \Gamma h \overline{u}^2 \\ \displaystyle\int_{z_b}^{\eta} uv dz = \Gamma h \overline{u}\,\overline{v} \\ \displaystyle\int_{z_b}^{\eta} v^2 dz = \Gamma h \overline{v}^2 \end{cases} \tag{23}$$

  with $\Gamma = 1$ for a vertical velocity profile, $\Gamma = 4/3$ a linear velocity profile and $\Gamma = 6/5$ a parabolic or semi-parabolic velocity profile. Theses results are classical and we refer to [Lavalle, 2014] for instance.

- The Coriolis effect introduces an integration over a portion of the thickness of the film $\int_z^{\eta^-} v dz$, which can not be solved exactly. To do so, we neglect the fluctuations terms, which leads to:

$$\int_z^{\eta^-} v dz = \overline{v}\,(\eta - z) \tag{24}$$

- The Coriolis effect also leads to the unknown term $\overline{w}$. Thanks to the continuity equation and, once again, by neglecting the fluctuations terms, we get:

$$\overline{w} = -\frac{h}{2}\left(\frac{\partial \overline{u}}{\partial x} + \frac{\partial \overline{v}}{\partial y}\right) \tag{25}$$

2.4 Closed form of the film model

The general closed form of the film model proposed in this paper is the system of equations (26) associated with the closure laws detailed paragraph 2.3 and the boundary conditions (equations (1), (4) and (16)) and is written:

$$\begin{cases} \dfrac{\partial h}{\partial t} + \dfrac{\partial h\overline{u}}{\partial x} + \dfrac{\partial h\overline{v}}{\partial y} = \mathcal{S}_h \\ \\ \dfrac{\partial h\overline{u}}{\partial t} + \dfrac{\partial}{\partial x}\left(\Gamma h\overline{u}^2 + \dfrac{g\cos\theta h^2}{2}\right) + \dfrac{\partial \Gamma h\overline{u}\,\overline{v}}{\partial y} + 2\omega_0\left(\overline{v}h\dfrac{\partial \eta}{\partial x} + \dfrac{h^2}{2}\dfrac{\partial \overline{v}}{\partial x}\right) - \dfrac{\omega_0^2}{2}h\dfrac{\partial \eta^2}{\partial x} = \\ -\dfrac{h}{\rho}\dfrac{\partial \mathscr{P}_g}{\partial x} - \dfrac{\sigma h}{\rho}\dfrac{\partial \mathscr{R}^{-1}}{\partial x} - hg\cos\theta\dfrac{\partial z_b}{\partial x} + \dfrac{1}{\rho}\left(\tau_{xz-r|_\eta} - \tau_{xz-r|_{z_b}}\right) + \left(\dfrac{\overline{u}+u_g}{2}\right)\mathcal{S}_h \\ \\ \dfrac{\partial h\overline{v}}{\partial t} + \dfrac{\partial \Gamma h\overline{u}\,\overline{v}}{\partial x} + \dfrac{\partial}{\partial y}\left(\Gamma h\overline{v}^2 + \dfrac{g\cos\theta h^2}{2}\right) + 2\omega_0\left(\overline{v}h\dfrac{\partial \eta}{\partial y} + \dfrac{h^2}{2}\dfrac{\partial \overline{v}}{\partial y}\right) - \dfrac{\omega_0^2}{2}h\dfrac{\partial \eta^2}{\partial y} + \omega_0 h^2\left(\dfrac{\partial \overline{u}}{\partial x} + \dfrac{\partial \overline{v}}{\partial y}\right) = \\ g\sin\theta h - \dfrac{h}{\rho}\dfrac{\partial \mathscr{P}_g}{\partial y} - \dfrac{\sigma h}{\rho}\dfrac{\partial \mathscr{R}^{-1}}{\partial y} - hg\cos\theta\dfrac{\partial z_b}{\partial y} + h\omega_0^2(r+y) + 2\omega_0 h\left(\overline{u}\dfrac{\partial z_b}{\partial x} + \overline{v}\dfrac{\partial z_b}{\partial y}\right) \\ + \dfrac{1}{\rho}\left(\tau_{yz-r|_\eta} - \tau_{yz-r|_{z_b}}\right) + \left(\dfrac{\overline{v}+v_g}{2}\right)\mathcal{S}_h \end{cases} \tag{26}$$

From now on, the Stator model (respectively the Rotor model) will refer to $\omega_0 = 0$ (respectively to $\omega_0 \neq 0$).

2.5 Model's properties

Properties of model (26) are now examined. These properties have multiple consequence: they enable to choose a suitable numerical scheme (conservativity and hyperbolicity), analytical solutions can be obtained to verify the code (entropy criteria and jump relations); they also give us clues on the relevance of the models (entropy criteria and invariances). These calculations can be found in chapter 3 of [Simon, 2017] and the results are summed up here in table 2.

	Stator model	**Rotor model (with $\Gamma = 1$)**
Conservative form	yes	no
Hyperbolicity	if $g\cos\theta > 0$	if $g\cos\theta + 2\omega_0\overline{v} - \omega_0^2 z_b > 0$
Entropy inequality	if $\Gamma = 1$	yes
Convex entropy	if $g\cos\theta > 0$	if $g\cos\theta - \omega_0^2\eta > 0$
Galilean invariance	if $\Gamma = 1$	$\times$
Rotational invariance w.r.t (x, y)	without condition	$\times$

Table 2: Properties of the Stator model and the Rotor model

The model obviously losses its conservative structure when the rotation is accounted for. The Stator model is hyperbolic only if the film is on the top of the wall. In this case, the gravity has a stabilizing effect on the film. When the film is under the wall, the gravity has a destabilizing effect and tends to release the film from the wall. This property is similar to the classical Shallow-Water equations. The addition of the rotation renders the hyperbolicity condition more intricate. The latter criteria may be compared to the work of [Tort et al., 2014]. For a liquid film in steam turbines, the situation where the model is not hyperbolic because of the gravity is likely to occur, however, it is unlikely that the rotation will be the cause of the loss of hyperbolicity. An entropy - flux entropy couple can be found when $\Gamma = 1$; thus the model can be controlled for $\Gamma = 1$. The model is Galilean invariant, that is to say that the equations in a none-moving frame of reference are similar to the equations in a frame of reference in uniform translation, when $\Gamma = 1$ only. These last two results can also be found in [Richard and Gavrilyuk, 2012]. The Stator model is invariant under rotation frame of a constant angle without any condition.

3 NUMERICAL METHOD

The 2D Stator model with $z_b = 0$ has been implemented in *Code_Saturne* code using a finite volume method on unstructured meshes. The different terms are solved with a fractional step method and the time step conditions on the discrete system are investigated.

3.1 Finite volume method

The Stator model with $z_b = 0$ can be written as follows:

$$\frac{\partial \underline{W}}{\partial t} + \nabla_{xy}.\left(\underline{\mathcal{F}}\left(\underline{W}\right)\right) = \underline{\mathcal{S}} + \underline{\mathcal{S}}_\sigma \tag{27}$$

with:

$$\underline{W} = \begin{pmatrix} h \\ h\overline{u} \\ h\overline{v} \end{pmatrix}; \qquad \underline{\mathcal{F}}_x\left(\underline{W}\right) = \begin{pmatrix} h\overline{u} \\ \Gamma h\overline{u}^2 + \dfrac{gcos\theta h^2}{2} \\ \Gamma h\overline{u}\ \overline{v} \end{pmatrix}; \qquad \underline{\mathcal{F}}_y\left(\underline{W}\right) = \begin{pmatrix} h\overline{v} \\ \Gamma h\overline{u}\ \overline{v} \\ \Gamma h\overline{v}^2 + \dfrac{gcos\theta h^2}{2} \end{pmatrix} \tag{28}$$

and:

$$\underline{\mathcal{S}} = \begin{pmatrix} \mathcal{S}_h \\ -\dfrac{h}{\rho}\dfrac{\partial \mathscr{P}^g_{|h^+}}{\partial x} + \dfrac{1}{\rho}\left(\tau_{xz-r|_\eta} - \tau_{xz-r|_0}\right) + \left(\dfrac{\overline{u} + u_g}{2}\right)\mathcal{S}_h \\ g\sin\theta h - \dfrac{h}{\rho}\dfrac{\partial \mathscr{P}^g_{|h^+}}{\partial y} + \dfrac{1}{\rho}\left(\tau_{yz-r|_\eta} - \tau_{yz-r|_0}\right) + \left(\dfrac{\overline{v} + v_g}{2}\right)\mathcal{S}_h \end{pmatrix}; \qquad \underline{\mathcal{S}}_\sigma = \begin{pmatrix} 0 \\ -\dfrac{\sigma h}{\rho}\dfrac{\partial \mathscr{R}^{-1}}{\partial x} \\ -\dfrac{\sigma h}{\rho}\dfrac{\partial \mathscr{R}^{-1}}{\partial y} \end{pmatrix} \tag{29}$$

By integrating the continuous expression (27) on a volume cell Ω_i and between two instants t^n and t^{n+1}, the finite volume scheme reads, using an explicit formulation for convective fluxes:

$$\left(\underline{W}_i^{n+1} - \underline{W}_i^n\right)\Omega_i + \Delta t^n \sum_{j\in\mathcal{V}(i)} \underline{\mathcal{F}}_{n,ij}^{\Delta x}\left(\underline{W^n}\right) S_{ij} = \Delta t^n \Omega_i \underline{\mathcal{S}}_i^{n+1} + \Delta t^n \int_{\Omega_i} \underline{\mathcal{S}}_\sigma d\Omega_i \tag{30}$$

where $\mathcal{V}(i)$ refers to the set of neighbors of cell i. We note $\Delta t^n = t^{n+1} - t^n$. The notation ij refers to the interface between cell i and cell j, S_{ij} is the surface of the interface between cells i and j, and the normal vector pointing outside is $\underline{n} = (n_x, n_y)^T$. We also note $\underline{\mathcal{F}}_n\left(\underline{W}\right) = n_x \underline{\mathcal{F}}_x\left(\underline{W}\right) + n_y \underline{\mathcal{F}}_y\left(\underline{W}\right)$. The time integration is achieved using a first order Euler scheme which can be extended to second order (Runge-Kutta).

3.2 Fractional step

The fractional step method consists in solving three distinct parts: convective effects, source terms and surface tension contribution.

3.2.1 Convective effects

The first fractional step goes from t^n to t^* and accounts for the convection contributions:

$$\Omega_i \underline{W}_i^* = \Omega_i \underline{W}_i^n - \Delta t^n \sum_{j\in V(i)} \underline{\mathcal{F}}_{n,ij}^{\Delta x}\left(\underline{W^n}\right) S_{ij} \tag{31}$$

A classical first order Rusanov scheme is used, together with the standard minmod limiter method (MUSCL type) in order to get a second order convergence rate. We thus write:

$$\underline{\mathcal{F}}_{n,ij}^{\Delta x}\left(\underline{W^n}\right) = \frac{1}{2}\left(\underline{\mathcal{F}}_n\left(\underline{W}_i^n\right) + \underline{\mathcal{F}}_n\left(\underline{W}_j^n\right) - \rho_{s,ij}^n\left(\underline{W}_j^n - \underline{W}_i^n\right)\right) \tag{32}$$

with the spectral radius $\rho_{s,ij}^n$ defined as follows:

$$\rho_{s,ij}^n = \max\left(\rho_{s,i}^n, \rho_{s,j}^n\right) \tag{33}$$

with in particular for the Stator model (where $\Gamma \geq 1$):

$$\rho_{s,i}^n = \rho_s\left(\frac{\partial \underline{\mathcal{F}}\left(\underline{W}_i^n\right)}{\partial \underline{W}}\right) = \Gamma |U_n|_i^n + c_i^n \sqrt{1 + \Gamma\left(\Gamma - 1\right)\left(M_i^n\right)^2} \tag{34}$$

where $M = U_n/c$ denotes the Mach number, $U_n = n_x\overline{u} + n_y\overline{v}$ is the normal velocity and the celerity is $c = \sqrt{gcos\theta h}$. Out of scope here, the eigenvalues for the Rotor model are given in section 3.2.2 of [Simon, 2017].

3.2.2 Source term

The second fractional step, described between the time t^* and t^{**}, handles the source terms $\underline{\mathcal{S}}$ in a implicit way. The general form of this step is:

$$\underline{W}_i^{**} = \underline{W}_i^* + \Delta t^n \underline{\mathcal{S}}\left(\underline{W}_i^{**}\right) \tag{35}$$

As the mass transfer is an external data, the explicitation of the continuity equation is straight:

$$h_i^{**} = h_i^* + \Delta t^n \mathcal{S}_h\left(\underline{W}_i^{**}\right) \tag{36}$$

The implicit momentum equation in the x-direction results in:

$$(h\overline{u})_i^{**} = \frac{(h\overline{u})_i^* + \Delta t^n\left(-\frac{h_i^{**}}{\rho}\left(\frac{\partial \mathscr{P}_g}{\partial x}\right)_i^{**} + F_{x,i,sl}^{**} u_{g,i}^{**} + \frac{u_{g,i}^{**}}{2}\mathcal{S}_{h,i}^{**}\right)}{1 + \Delta t^n\left(\frac{F_{x,i,sl}^{**}}{h_i^{**}} + \frac{c_{f,w}^*}{2}\frac{\left(h\,|\overline{u}|\right)_i^*}{h_i^* h_i^{**}} - \frac{\mathcal{S}_{h,i}^{**}}{2h_i^{**}}\right)} \tag{37}$$

with:

$$F^{**}_{x,i,sl} = \frac{\rho^{**}_{g,i}}{\rho}\frac{c_{f,int}}{2}\left|u^{**}_{g,i} - \left(\frac{h\overline{u}}{h}\right)^{*}_{i}\right| \tag{38}$$

if $\mathcal{S}^{**}_{h,i} < 0$. A similar expression is used for the component v of the velocity.

When $\mathcal{S}^{**}_{h,i}$ is positive a different scheme for the expression (37) can ensure an unconditional definition of $(h\overline{u})^{**}_i$ which is written as follows:

$$(h\overline{u})^{**}_i = \frac{Sg(\mathcal{S}^{**}_{h,i})\,(h^{**}_i\overline{u}^{*}_i) + \left(1 - Sg(\mathcal{S}^{**}_{h,i})\right)(h\overline{u})^{*}_i + \Delta t^n\left(-\frac{h^{**}_i}{\rho}\left(\frac{\partial \mathscr{P}^{g}_{|h^+}}{\partial x}\right)^{**}_i + F^{**}_{x,i,sl}u^{**}_{g,i} + \frac{u^{**}_{g,i}}{2}\mathcal{S}^{**}_{h,i}\right)}{1 + \Delta t^n\left(\frac{F^{**}_{x,i,sl}}{h^{**}_i} + \frac{c^{*}_{f,paroi}}{2}\frac{(h\,|\overline{u}|)^{*}_i}{h^{*}_i h^{**}_i} + \frac{|\mathcal{S}^{**}_{h,i}|}{2h^{**}_i}\right)} \tag{39}$$

with the function $Sg(X)$ defined such as:

$$Sg(X) = \begin{cases} 1 & \text{if } X > 0 \\ 0 & \text{if } X \leq 0 \end{cases} \tag{40}$$

3.2.3 Surface tension

The third fractional step goes from t^{**} to t^{n+1} and deals with the surface tension. The surface tension is numerically delicate to handle as it involves a third order derivative. In a first approach, the surface tension is implemented in one dimension with a classical centered scheme:

$$\Omega_i \underline{W}^{n+1}_i = \Omega_i \underline{W}^{**}_i + \Delta t^n \int_{\Omega_i} \underline{\mathcal{S}}_\sigma d\Omega \tag{41}$$

with $\underline{\mathcal{S}}_\sigma = \left(0, 0, \frac{\sigma h}{\rho}\frac{\partial^3 h}{\partial y^3}\right)^T$

By stating that the space step Δy is constant, we choose to implicit the surface tension as follows:

$$(h\overline{v})^{n+1}_i = (h\overline{v})^{**}_i + \frac{\Delta t^n}{2\Delta y^3}\frac{\sigma}{\rho}h^{n+1}_i\left(h^{n+1}_{i+2} - 2h^{n+1}_{i+1} + 2h^{n+1}_{i-1} - h^{n+1}_{i-2}\right) \tag{42}$$

Three classical boundary conditions are used: wall boundary conditions (using the mirror state technique), homogeneous Neumann or periodic boundary conditions for inlet/outlet.

3.3 Time step restriction

Constraints on time step are enforced to guarantee the positivity of the film height and to ensure the stability of the scheme.

3.3.1 Positivity of the film height

In the first step, dealing with the convection effects, the discrete mass balance equation can be reorganized as follows :

$$h^{*}_i\Omega_i = h^n_i\left(\Omega_i - \frac{\Delta t^n}{2}\sum_{j\in V(i)}\left(u^n_i.n_{ij} + \rho^n_{s,ij}\right)S_{ij}\right) + \frac{\Delta t^n}{2}\sum_{j\in V(i)}h^n_j\left(\rho^n_{s,ij} - u^n_j.n_{ij}\right)S_{ij} \tag{43}$$

Thus assuming that h^*_i are being positive, a necessary and sufficient condition is that h^*_i should be a convex combination of the h^n_j, such that:

$$\begin{cases} \rho^n_{s,ij} - u^n_j.n_{ij} > 0 \\ \Omega_i - \dfrac{\Delta t^n}{2}\displaystyle\sum_{j\in V(i)}\left(u^n_i.n_{ij} + \rho^n_{s,ij}\right)S_{ij} > 0 \end{cases} \tag{44}$$

The first condition is always fulfilled by Rusanov scheme. The second condition restricts the time step and is classically called the CFL condition:

$$\Delta t^n = \frac{2\Omega_i CFL}{\sum\limits_{j\in V(i)} \left(u_i^n.n_{ij} + \rho_{s,ij}^n\right) S_{ij}} = \frac{2\Omega_i CFL}{\sum\limits_{j\in V(i)} \rho_{s,ij}^n S_{ij}} \tag{45}$$

since

$$\sum_{j\in V(i)} u_i^n.n_{ij} S_{ij} = 0 \tag{46}$$

where $0 < CFL < 1$.

The second fractional step links the film height to the mass source term such that:

$$\left(h_i^{**} - h_i^*\right)\Omega_i = \Delta t^n \Omega_i \mathcal{S}_h \tag{47}$$

We recall that $\mathcal{S}_h > 0$ corresponds to droplet deposition and $\mathcal{S}_h < 0$ represents evaporation. In order to ensure the positivity of the film height we must have $\Delta t^n > -h_i^*/\mathcal{S}_h$. This relation is always true for $\mathcal{S}_h$ independent from h and positive which corresponds to the droplet deposition.

3.3.2 Stability of numerical scheme

By performing a von Neumann stability analysis of the numerical scheme, we can obtain a stability condition depending on the surface tension as well as a condition on the convection similar to the condition to ensure the positivity of the film height (expression (45)). Appendix B details the calculation with the first order Rusanov scheme which are mandatory to get this condition. This results in:

$$\max\left(\frac{\Delta t}{\Delta x}\rho_s\left(\underline{\underline{C}}\right), \frac{\Delta t}{\Delta x}\rho_s\left(\underline{\underline{C}}\right)\left(\frac{|u_0| + \sqrt{c_0^2 + \dfrac{4\sigma h_0}{\rho(\Delta x)^2}}}{\rho_s\left(\underline{\underline{C}}\right)}\right)^2\right) \leq 1 \tag{48}$$

with $c_0 = \sqrt{g\cos\theta h_0}$ for the classical Shallow-Water equation and the Stator model and $\rho_s\left(\underline{\underline{C}}\right)$ the spectral radius of the Jacobian matrix of the flux.

The second-order Rusanov scheme at order 2 MUSCL type discretization and a second order Runge-Kutta scheme leads to the following restriction on the time step:

$$\Delta t^n \leq \frac{7^{7/6}\sqrt{3}}{24}\left(\frac{\rho\sqrt{\bar{v}_0 + c_0}}{\sigma h_0}\right)^{2/3}\Delta y^{7/3} \tag{49}$$

Compared to the study of [Noble and Vila, 2014], the restrictions at order 1 and at order 2 are performed in dimensional variables.

Remark:
In [Simon et al., 2016] and in chapter 5 of [Simon, 2017], several verifications of the numerical schemes are made to ensure that convergence is reached w.r.t. the mesh size. Analytical solutions for the test cases of the dam break (particular Riemann problem), a lake at rest and the deposition on a plane are obtained and compared to numerical simulations.

4 NUMERICAL RESULTS

4.1 Falling film

In this section, the model equation (26) is validated for a falling film. These falling films are compared to the experiments of [Liu and Gollub, 1994]. In these particular situations, the model developed in this paper

(expression (26)) degenerates into the Shallow-Water equations with surface tension. Indeed, for a film flowing down a plane, there is no rotation, no mass transfer, no free surface shear and the gas pressure as well as the position of the wall z_b are constants. It is indeed a one dimensional case and we set $\Gamma = 1$. The resulting model used in the section includes the convection, the gravity, the friction at the wall (expression (15)) and the surface tension. It may be rewritten as:

$$\begin{cases} \dfrac{\partial h}{\partial t} + \dfrac{\partial h\overline{v}}{\partial y} = 0 \\ \dfrac{\partial h\overline{v}}{\partial t} + \dfrac{\partial}{\partial y}\left(h\overline{v}^2 + \dfrac{g\cos\theta h^2}{2}\right) = g\sin\theta h - \dfrac{3\nu\overline{v}}{h} + \dfrac{\sigma}{\rho}h\dfrac{\partial^3 h}{\partial y^3} \end{cases} \tag{50}$$

More generally, these simulations also enable to judge the precision of a relative simple model which is also the Shallow-Water equations with surface tension (equation (50)) for a falling film test case. These simulations will be compared to those resulting from the application of more sophisticated models such as the model of [Ruyer-Quil and Manneville, 2000] and the model of [Lavalle, 2014].

4.1.1 Falling film in linear regime

Under certain circumstances, a falling film on inclined plane displays waves at the free surface. These waves come from an amplification of a small perturbation. The evolution of the perturbation depends on the Reynolds number of the liquid film (or the Froude number). A infinitesimal perturbation is amplified (respectively damped) if the Reynolds number of the liquid film is greater than (respectively smaller than) a critical Reynolds number. A linear stability analysis of the Navier–Stokes equations provides an estimation of this critical Reynolds number. This one is based on the inclination angle θ of the plane ($\theta = 0$ corresponds to a horizontal plane, see figure 4):

$$Re_{cr-NS} = \frac{5}{6}\operatorname{cotan}\theta \tag{51}$$

This critical Reynolds number has been validated by the experimental result of [Liu and Gollub, 1994]. The models of [Ruyer-Quil and Manneville, 2000], [Lavalle, 2014] or [Richard et al., 2016] are built in order to comply with this critical Reynolds number.

A stability analysis is performed on the Stator model equation (50) which corresponds to the Shallow-Water equations with surface tension. This analysis can be found in appendix C and shows the same results for two different linearizations. It leads to a different bifurcation threshold than the expression (51), which reads:

$$Re_{cr-Stator} = \frac{3}{4}\operatorname{cotan}\theta \tag{52}$$

In order to verify the numerical approach, we introduce some perturbations in the linear regime. Thus, we simulate a film on a plane inclined with a initial perturbation in the form:

$$\begin{cases} h(y, t=0) = h_0(1 + \epsilon\sin(2\pi\dfrac{y}{\lambda})) \\ \overline{v}(y, t=0) = v_0(1 + \epsilon\sin(2\pi\dfrac{y}{\lambda})) \end{cases} \tag{53}$$

where $\epsilon = 10^{-6}$ enables to remain in the linear regime, and $h_0/\lambda << 1$ in order to remain in the long-wave domain (condition to obtain the analytical threshold expression (52)). The fluid is chosen in agreement with the experiment of [Liu and Gollub, 1994]: a glycerin solution is considered with density $\rho = 1070\ kg/m^3$, kinematic viscosity $\nu = 6.28 \times 10^{-6}\ m^2/s$ and surface tension coefficient $\sigma = 0.067\ N/m$. Unlike in the experiment of [Liu and Gollub, 1994], the Reynolds number of the film is not defined with the velocity at the free surface but with the average flow velocity. The height is in both cases the height of the mean or undisturbed flow: $Re = h_0 v_0/\nu$. The Weber number is defined as $We = \rho h_0 v_0^2/\sigma$ and the Froude number is defined such that $Fr = v_0/\sqrt{g h_0}$.

The plane inclination angle θ is 6.4 degrees in accordance with the experiment. The resulting analytical critical Reynolds number of the Stator model is 6.69 using expression (52), whereas the one predicted by equation (51) is 7.43. Computational results for different meshes are given in table 3. If the initial perturbation is amplified,

Cells number \ Reynolds of the film	7.82	7.91	8.00	8.08	8.17	8.26	8.52	8.95
100	ST	ST	ST	ST	ST	ST	ST	**UN**
500	ST	ST	ST	ST	ST	**UN**	UN	UN
1000	ST	ST	ST	**UN**	UN	UN	UN	UN
2000	ST	**UN**	UN	UN	UN	UN	UN	UN

Table 3: Stability of the film compared to the Reynolds of the film for different meshes for the Stator model where $Re_{cr-Stator} = 6.69$

the film is considered as unstable ("UN"), whereas if the initial perturbation is damped, the film is considered as stable ("ST"). The color underlines an approximation of the limit between the stable case and the unstable case for the Stator model (50). In his thesis, [Lavalle, 2014] proceeds to the same numerical test with meshes up to 160 cells. Considering table 3, we see that the numerical threshold is less than 7.91 for the Stator model, since the code gets closer to the analytical solution for finer meshes. The model together with the numerical scheme has the expected threshold behavior.

4.1.2 Falling film in non-linear regime

[Liu and Gollub, 1994] observed nonlinear instabilities at the free surface of a thin film flowing on an inclined plane by periodically forcing the film at the inlet. They conclude that the nonlinear development of these waves depends on the frequency of forcing. After the study of the mesh convergence and a sensitivity study of the forcing amplitude, we will compare the shape of these waves with the Stator model (50) and the two reference models: [Ruyer-Quil and Manneville, 2000] model and the [Lavalle, 2014] model. [Ruyer-Quil and Manneville, 2000] first order model is recalled here:

$$\begin{cases} \dfrac{\partial h}{\partial t} + \dfrac{\partial q}{\partial y} = 0 \\ \dfrac{\partial q}{\partial t} + \dfrac{17}{7}\dfrac{q}{h}\dfrac{\partial q}{\partial y} + \left(\dfrac{5}{6}g\cos\theta h - \dfrac{9}{7}\dfrac{q^2}{h^2}\right)\dfrac{\partial h}{\partial y} = \dfrac{5}{6}gh\sin\theta - \dfrac{5}{2}\dfrac{q}{h^2} + \dfrac{5}{6}\dfrac{\sigma}{\rho}h\dfrac{\partial^3 h}{\partial y^3} \end{cases} \tag{54}$$

as well as [Lavalle, 2014] model:

$$\begin{cases} \dfrac{\partial h}{\partial t} + \dfrac{\partial q}{\partial y} = 0 \\ \dfrac{\partial q}{\partial t} + \dfrac{\partial}{\partial y}\left(\dfrac{q^2}{h} + \dfrac{1}{2}g\cos\theta h^2 + \dfrac{2}{225}\left(\dfrac{g\sin\theta}{\nu}\right)^2 h^5\right) = gh\sin\theta - \dfrac{3q}{h^2} + \dfrac{\sigma}{\rho}h\dfrac{\partial^3 h}{\partial y^3} \end{cases} \tag{55}$$

with $q = h\overline{v}$.

In order to agree with the conditions of the [Liu and Gollub, 1994] experiment, and owing to our definitions of the Reynolds number and the Weber number, these numbers must be equal to 19.33 and 0.184 respectively. Constant values of height and velocity such that $h_0 = 1.2791 \times 10^{-3}\ m$ and $v_0 = 9.49 \times 10^{-2}$ are enforced at the beginning of the computation. The inlet boundary condition represents the periodic perturbation and is defined as:

$$\begin{cases} h(y, t = 0) = h_0(1 + \epsilon\sin(2\pi t f_{req})) \\ \overline{v}(y, t = 0) = v_0(1 + \epsilon\sin(2\pi t f_{req})) \end{cases} \tag{56}$$

where f_{req} denotes the forcing frequency ($1.5\ Hz$ or $4.5\ Hz$ given by the experiment) and $\epsilon = 10^{-3}$ (a sensitive analysis of ϵ is carried on further). The outlet boundary condition is a homogeneous Neumann condition.

Figure 6 displays the effects of mesh refinement for the Stator model (50). A further mesh dependence analysis of the film height and the wavelength for the Stator model as well as for the model of [Ruyer-Quil and Manneville, 2000]

and [Lavalle, 2014] is presented in section 6.2.1 of [Simon, 2017]. We note that capillary waves are not captured with a mesh of 1000 cells. Thereafter for this test case, all the simulations are carried with 8000 cells.

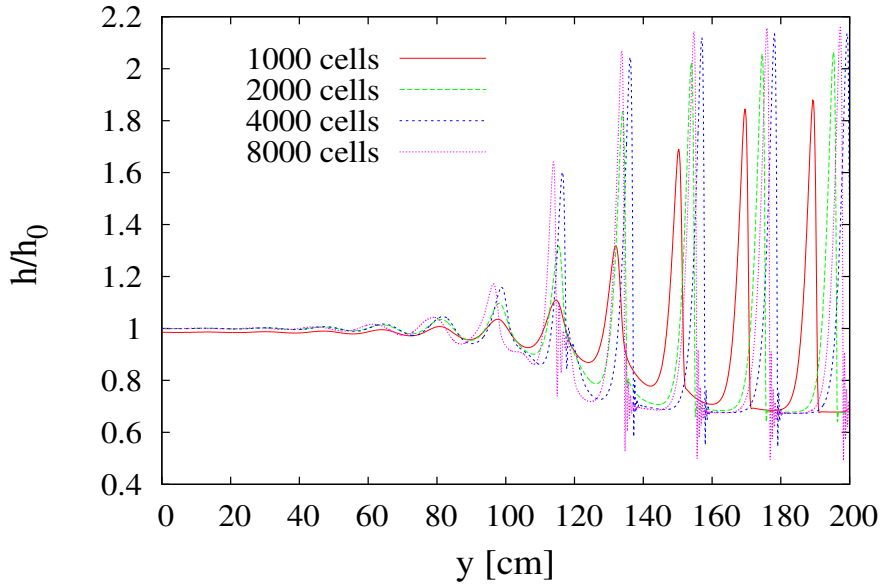

Figure 6: Relative height (h/h_0) for different meshes with a forcing frequency of 1.5 Hz for the Stator model at time $t = 12$ sec

In [Liu and Gollub, 1994] experiment, the forcing amplitude is not determined. This amplitude, denoted here by ϵh_0, intervenes in the boundary conditions described in equation (56). For a mesh of 8000 cells and a forcing frequency of 1.5 Hz, we can change the forcing amplitude ($\epsilon = 10^{-4}, 10^{-3}, 10^{-2}$) and observe the variations of the results figure 7. The results are given under established conditions.

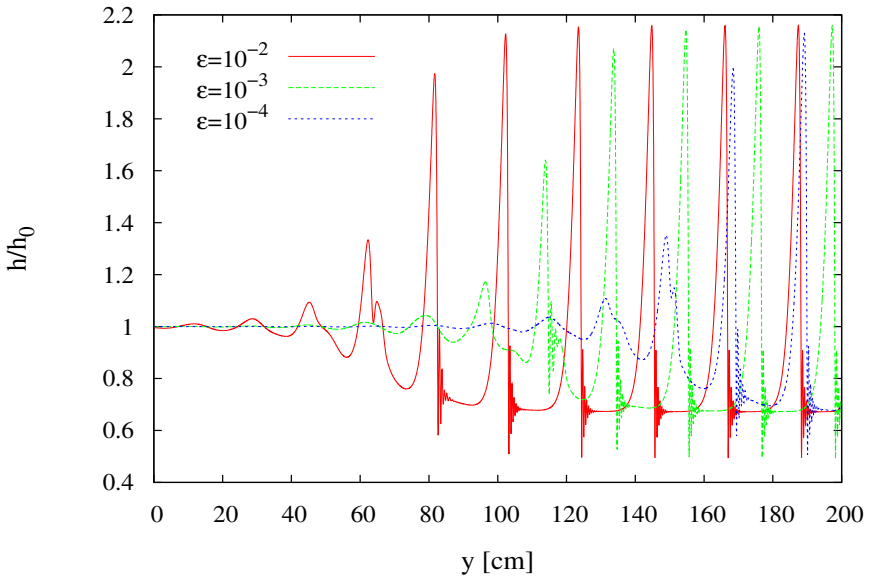

Figure 7: Relative height (h/h_0) as a function of y for different forcing amplitudes, with a frequency 1.5 Hz. Stator model with 8000 cells at time $t = 12$ sec

Figure 7 shows that the wavelength and the wave amplitude do not depend on the amplitude of forcing and can therefore be compared with the results of the experiment. Therefore, the forcing amplitude significantly influences the spatial point of development of the instabilities. The smaller the forcing amplitude, the greater the spatial point at which the established regime begins. However, the establishment distance can not be validated due to lack of experimental data. For the remaining simulations, we choose a forcing amplitude such that $\epsilon = 10^{-2}$.

Now, we compare the Stator model for two forcing frequencies (1.5 Hz and 4.5Hz) with the experience of [Liu and Gollub, 1994] and reference models for liquid films of [Ruyer-Quil and Manneville, 2000] and [Lavalle, 2014]. Figure 8 shows the experimental height with a forcing frequency of 1.5 Hz, for the three models. The simulations are performed with a forcing amplitude such that $\epsilon = 10^{-2}$ and a mesh size of 8000 cells. Figure 9 shows the results under the same conditions for a forcing frequency of 4.5 Hz. As mentioned in the previous section, since the starting point can not be reproduced due to lack of experimental data, we compare the dimensionless height on the same plate length (50 cm) without taking into account the value of the distance at the origin.

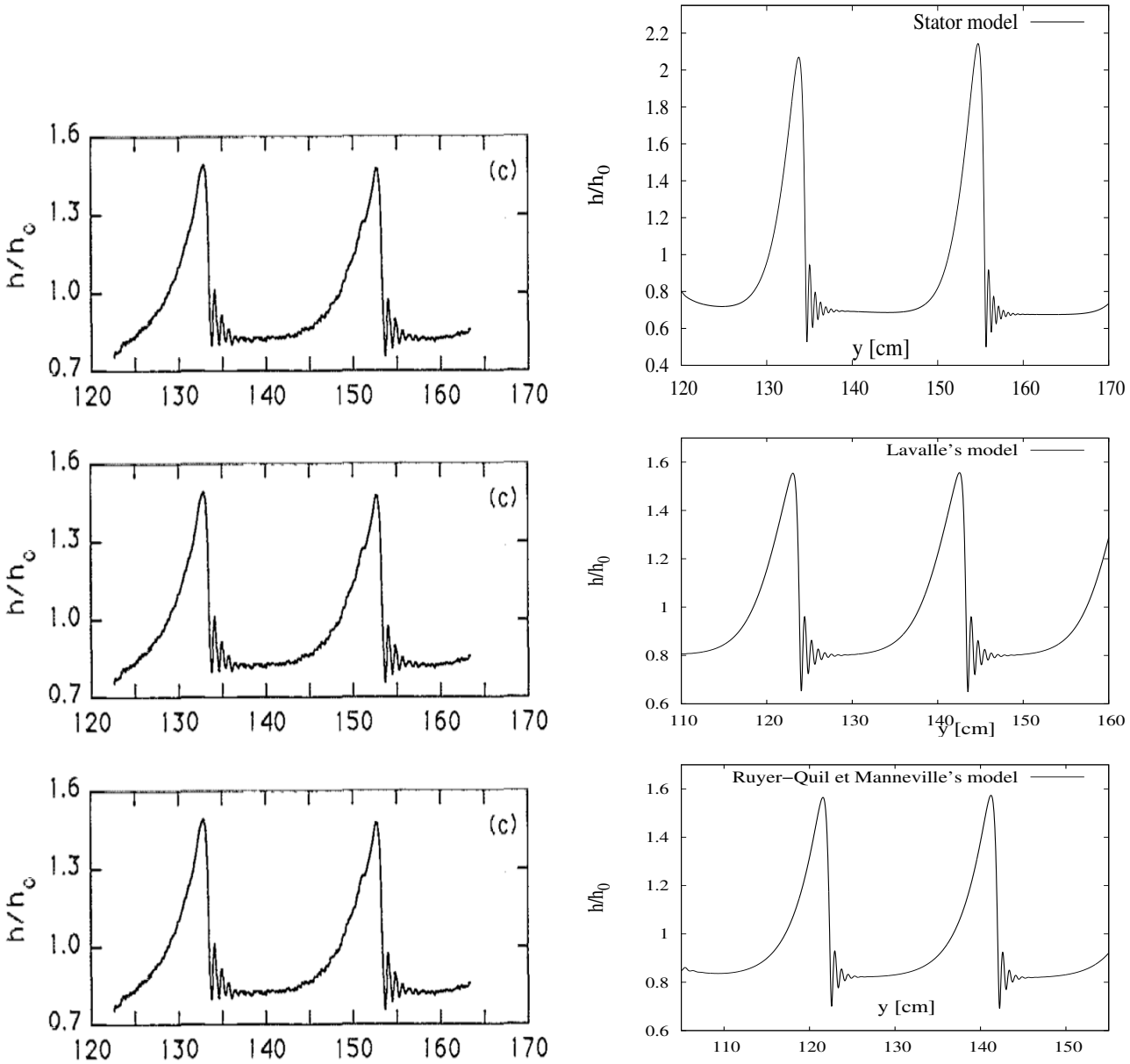

Figure 8: Behavior of falling liquid film solicited at 1.5 Hz. Left: results obtained by [Liu and Gollub, 1994] experiment. Right from top to bottom: results of the code with the Stator model, with the [Lavalle, 2014] model and with [Ruyer-Quil and Manneville, 2000] model with 8000 cells

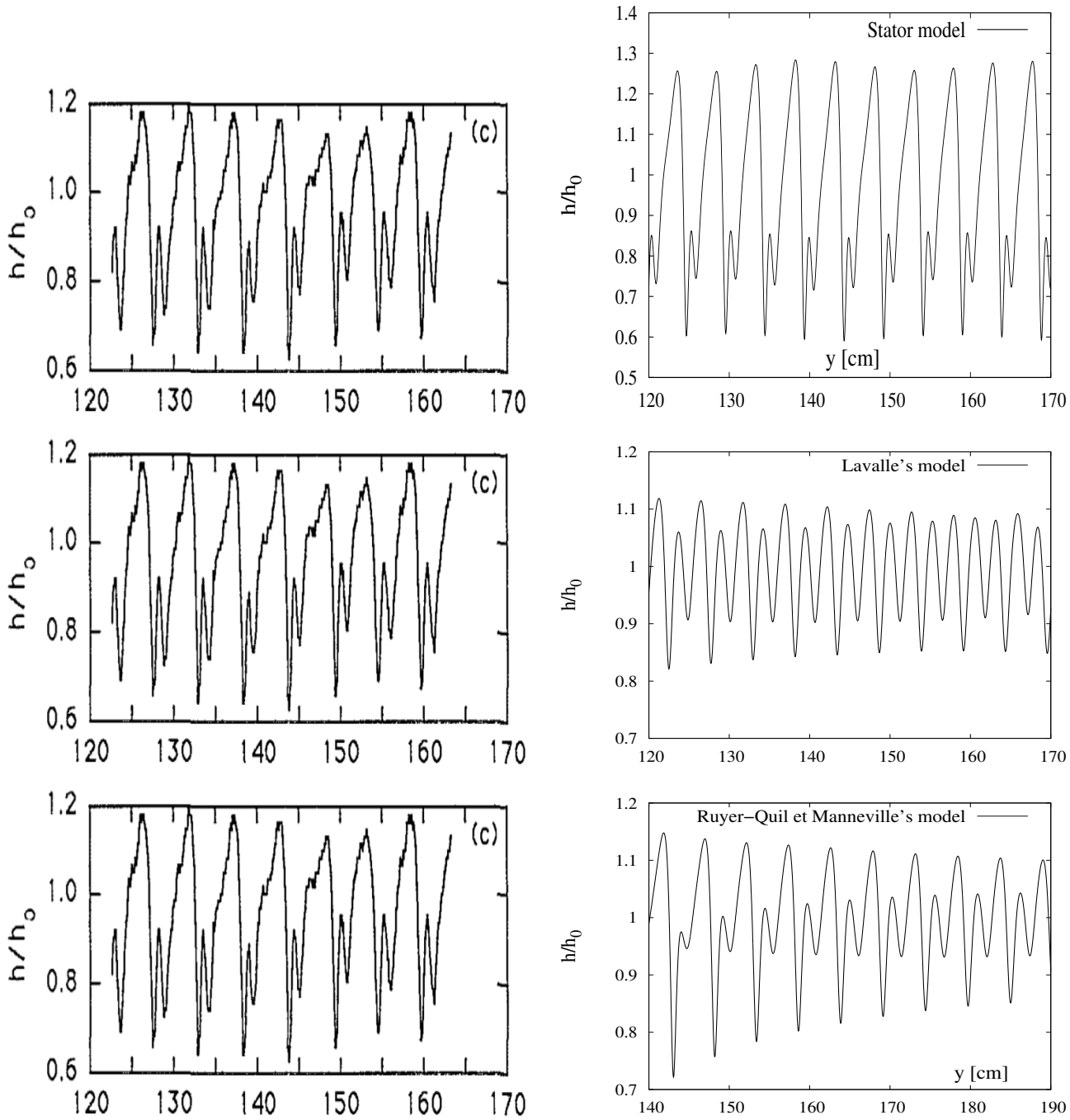

Figure 9: Behavior of a falling liquid film solicited at $4.5Hz$. Left: results obtained by [Liu and Gollub, 1994] experiment. Right from top to bottom: results of the code with the Stator model, with the [Lavalle, 2014] model and with the [Ruyer-Quil and Manneville, 2000] model with 8000 cells

[Ruyer-Quil and Manneville, 2000] model reproduces quantitatively the experiment for forcing frequencies 1.5 Hz and 4.5 Hz. Indeed, the maximum amplitudes of waves and the wavelengths are very close to the experiment. For the [Lavalle, 2014] model, the results for the 1.5 Hz forcing are quantitatively in agreement with the experiment but this is no longer true when the frequency is 4.5 Hz, since amplitude and wavelength of the waves are slightly underestimated. The wavelengths obtained with the Stator model, for the two forcing frequencies are also close to the experiment. However, the Stator model overestimates the wave amplitude of

about 30% for the forcing frequency 1.5 Hz and about 5% for the forcing frequency 4.5 Hz. The Stator model, or Shallow-Water model with the surface tension, therefore correctly reproduces the expected behavior of the free surface of a liquid film on a inclined plane and periodically forced.

4.2 Sheared film

In order to get closer to the real configuration of the liquid film in the steam turbines, simulations are performed with steam shear under steam turbine low-pressure conditions which means that the properties of the film and steam as well as steam velocity are realistic data for low-pressure turbine. In theses situations, the model degenerates as follows:

$$\begin{cases} \dfrac{\partial h}{\partial t} + \dfrac{\partial h\overline{v}}{\partial y} = \mathcal{S}_h \\ \dfrac{\partial h\overline{v}}{\partial t} + \dfrac{\partial}{\partial y}\left(h\overline{v}^2 + \dfrac{gh^2}{2}\right) = \dfrac{1}{\rho}\left(\tau_{yz-r|_h} - \tau_{yz-r|_0}\right) + \dfrac{\sigma}{\rho}h\dfrac{\partial^3 h}{\partial y^3} \end{cases} \tag{57}$$

The shear at the free surface $\tau_{yz-r|h}$ is modeled with the expression of [Spedding and Hand, 1997] (see expression (14)) and $\tau_{yz-r}|_0$ is modeled with the expression of [Ihnatowicz et al., 1979] (see equation (18)). First, a comparison of the model with the [Hammitt et al., 1981] experiment validates the stationary results. The unsteady features of the sheared film are then studied: on the one hand by imposing a frequency of the waves at the free surface of the film and on the other hand by forcing the film with a noise in order to capture the natural frequency of the film.

4.2.1 Steady sheared film

In the [Hammitt et al., 1981] experiment, liquid water is pumped vertically through a slot on a horizontal plate. The liquid film thus created is sheared by a steam flow at saturation and at high speed (60 m/s to 390 m/s) for both phases, the pressure and the temperature are 0.2 bar and 52.2 ℃ respectively.

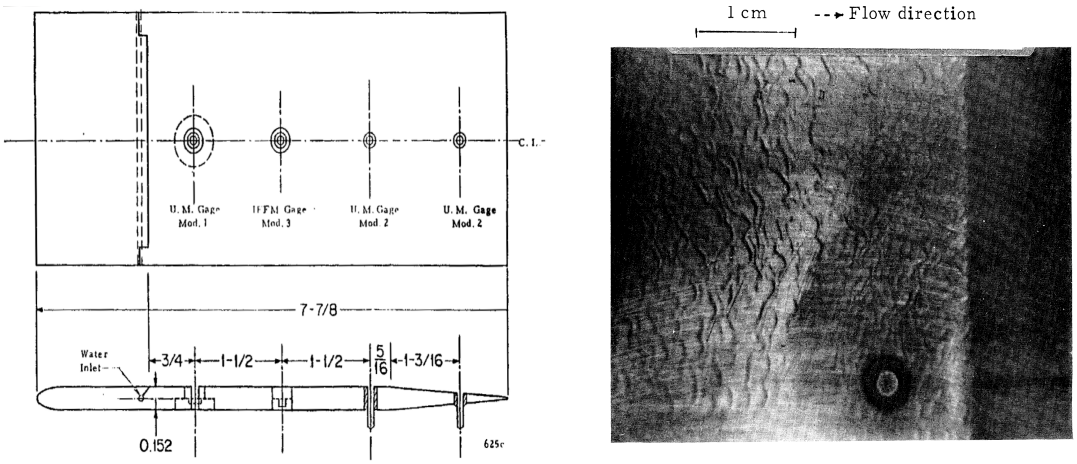

Figure 10: University of Michigan experimental setup (left) and typical observation with $v_g = 130\ m/s$ (right). Figures from [Hammitt et al., 1981]

A diagram of the experimental plate is presented as well as a typical observation of the liquid film with a steam velocity of 130 m/s. The wet dimensions of the plate are 133.3 mm in length (1) and 80 mm in width (L). The experimental results provide film heights as a function of the steam velocity for different liquid water flow rates under low pressure conditions. The heights of the film are given at four positions of the plate, as indicated in the figure by the sensors, and they are obtained using a temporal average.

Concerning the numerical procedure, the film height and velocity are initialized to zero. The mass transfer $\mathcal{S}_h$ transcribes the injection of liquid water through the slot of the flat plate. The value of the water flow used

is $\dot{m} = 5.10^{-7} m^3/s$. The flow rate of the experiment is converted into an additional water height at each time step such that:

$$\frac{h^{n+1} - h^n}{\Delta t} = \frac{\dot{m}}{lL(l_{inj}/100)} \tag{58}$$

with l_{inj} the slot length through which the flow is injected as a percentage of the length of the plate. The injection starts at 0.02 m and we have $l_{inj} = 5\%$. Since the code is using a fractional step method, convection does not appear in the expression (58). The properties of the liquid film and the vapor are calculated using the thermodynamic tables *IAPWS-IF97* ([Iapws,]) and are summarized as follows: density of film, $\rho = 983\ kg/m^3$, gas density $\rho_g = 9.5 \times 10^{-2}\ kg/m^3$, kinematic viscosity of the film, $\nu = 5.34 \times 10^{-7}\ m^2/s$, kinematic viscosity of the gas, $\nu_g = 1.11 \times 10^{-3}\ m^2/s$ and surface tension coefficient, $\sigma = 0.067\ kg/s^2$. As in the experiment, the heights are obtained by performing a temporal average.

A mesh convergence study is performed and can be found in section 7.3.1 of [Simon, 2017]: these stationary simulations are mesh independent with 100 cells.

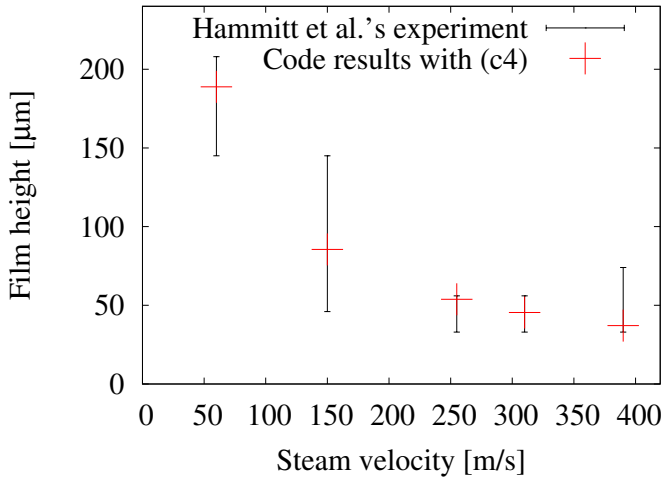

Figure 11: Time average of height for different steam velocities in the experiment (black bars) and with the numerical code (red crosses) with 100 cells

In figure 11, the results shows that the height decreases when the speed of the steam increases. The four experimental values on the plate remain within the black bars. As the numerical values are all within experimental range, the code presents fair results compared to the experiment.

4.2.2 Unsteady sheared film : mono-frequency forcing

We now study the Stator model, considering an unsteady test case that stages a liquid film on a horizontal plane which is forced at a given frequency at the entrance. First, it enables to emphasize the importance of surface tension in the description of waves at the interface of the film. It also makes it possible to investigate the behavior of the liquid film when sheared under unsteady conditions.

The model that is used is described by expression (57) and the properties of the fluids are derived from the Michigan experiment for liquid films in the low-pressure steam turbine conditions (see paragraph 4.2.1). We initialize the film at a constant height h_0 and the velocity v_0 is set to zero in a large domain (compared to the height of the film). The right boundary condition is a homogeneous Neumann condition and at the left boundary, the film evolves in time, simulating sinusoidal waves such as:

$$h(y = 0, t) = h_0(1 + \epsilon \sin(2\pi f t)) \tag{59}$$

ϵh_0 stands for the amplitude of the wave and f is the frequency of the wave. The flow parameters are typical values of this experiment: $h_0 = 100\ \mu m$, $\epsilon = 0.25$, $f = 10\ Hz$ and $v_g = 100\ m/s$.

A mesh sensitivity analysis is performed. A $t = 0$, the film velocity is zero. The film is set in motion with the steam drive. We compare the height and velocity of the film over the entire domain when the flow is established ($t = 1.8\ s$). We assume that the simulation results are almost converged on a mesh with 2000 cells, we will keep this mesh for all simulations.

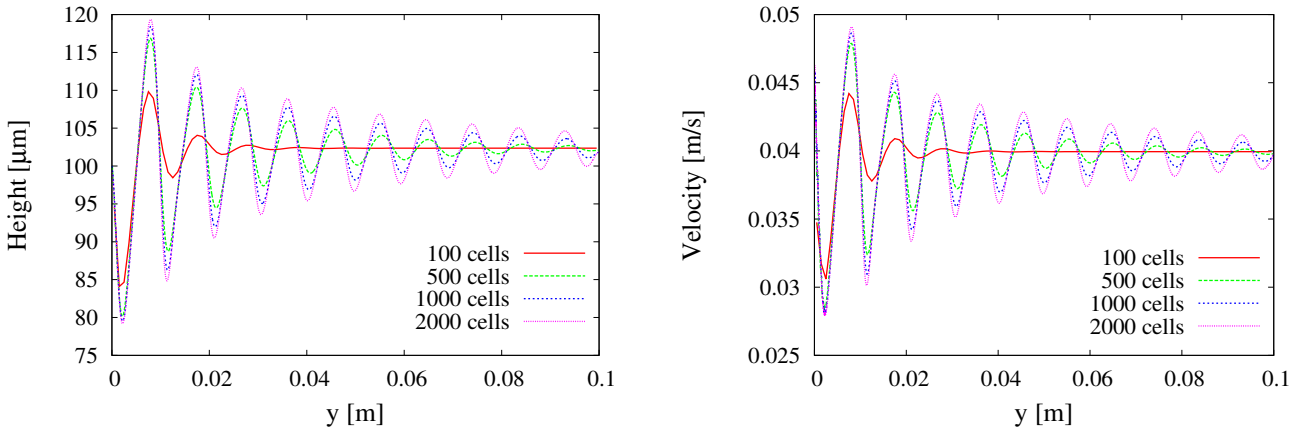

Figure 12: Mesh convergence of the height (left) and the velocity (right) of a film subjected to periodic input to low-pressure turbine conditions with $v_g = 100\ m/s$ at $t = 1.8\ s$

The height of the film with surface tension and without surface tension for a frequency imposed at the input of 10 Hz are displayed on figure 13, using an initial height of 100 μm and a steam speed of 100 m/s.

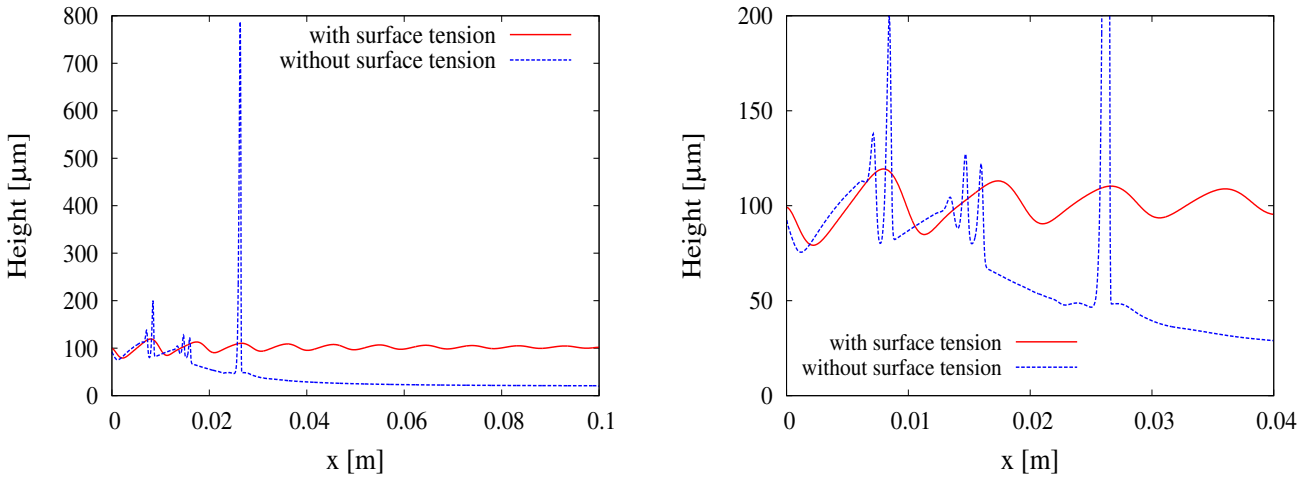

Figure 13: Study of the influence of surface tension: film height (left) and zoom (right) for 2000 cells $f = 10$ Hz, $v_g = 100\ m/s$ and $h_0 = 100\ \mu m$

Figure 13 exhibits the striking importance of surface tension effects for sheared films under turbine conditions. The surface tension smooths the peaks, which is expected since its expression depends on the curvature of the free surface. Therefore, the surface tension needs to be taken into account. Nonetheless, its discretization is CPU time consuming as the time step has to be strongly restricted for fine mesh (see appendix B). That explains why a distinct numerical approximation based on a change of variable $\varpi = h^{-1/2}\partial h/\partial y$ and a extension of the state variable $(h, h\overline{v}) \rightarrow (h, h\overline{v}, h\varpi)$ is sometimes used (see [Noble and Vila, 2014]). It has the advantage to decrease the derivative order of the system. Preliminary comparisons between the two approaches can be found in [Simon, 2017] (section 4.1.3 and 6.1.2) and shows similar results for a test case involving a falling film on a inclined plane.

We now vary the velocity of the steam in a typical turbine range and observe the height of the liquid film. The results are presented at $t = 1.8\ s$ in figure 14.

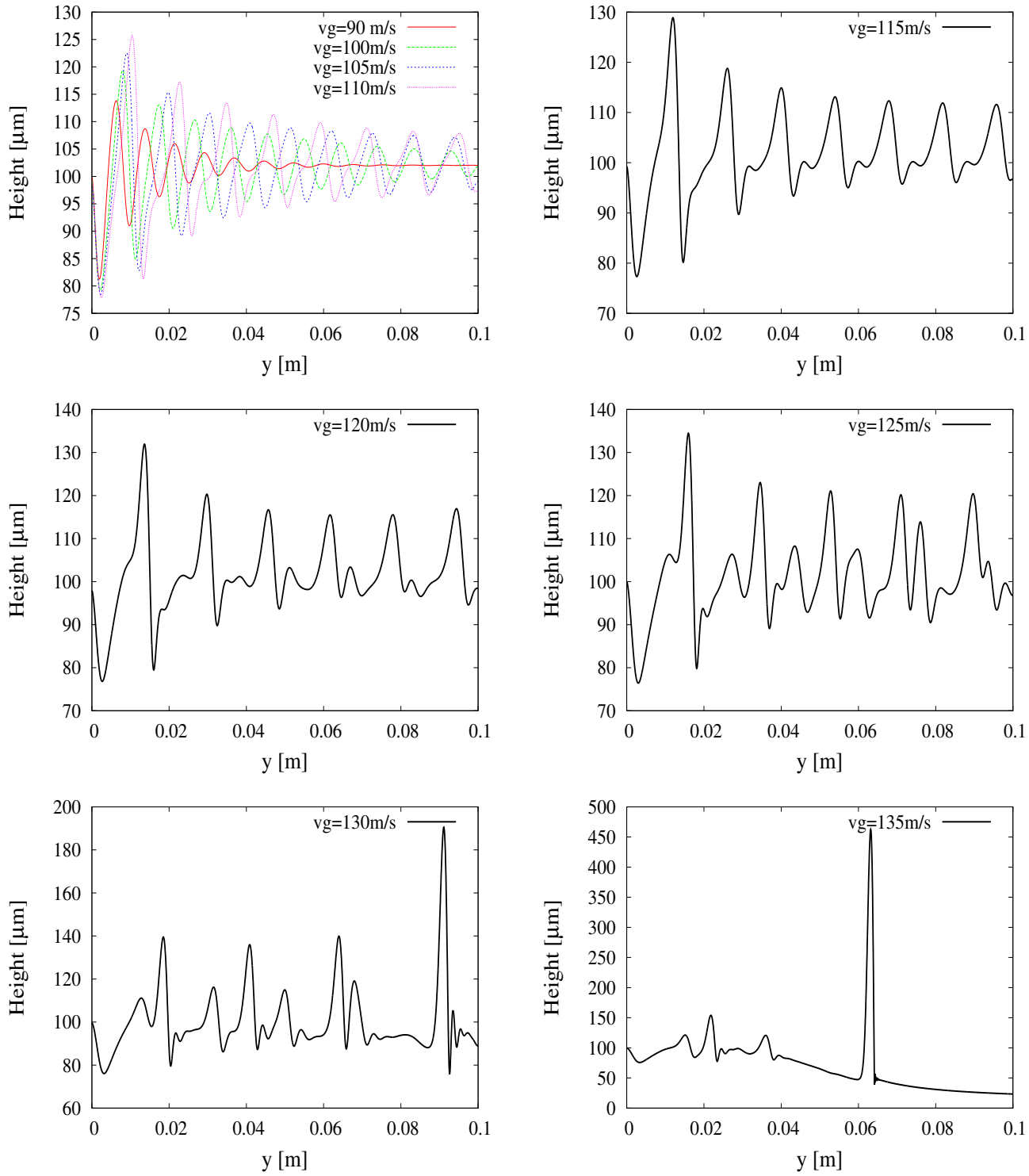

Figure 14: Height of the film with a frequency of forcing of 10 Hz for different steam velocities at $t = 1.8\ s$

For steam velocity from 90 m/s to 110 m/s, the flow is stable since the initial perturbation is attenuated.

It is noted that the speed of the film increases with the speed of the vapor. This tendency is explained simply because the steam drives the film with it. On the other hand, the increase of the gas velocity generates an increase in the wavelength of the waves at the interface of the liquid film and a decrease in the amplitude of these waves. The same feature was found by [Wurz, 1978] when he studied experimentally a film-gas co-current flow. For steam velocity below 110 m/s, the disturbance remains sinusoidal throughout the domain. Conversely, for a steam velocity of 110 m/s, the film changes its structure and adopts a non-sinusoidal profile.We also find that starting from $v_g = 115\ m/s$, the height of the peaks damps at the beginning and then seems to stabilize at a constant value, here at 111 μm. Until now the waves did not interact with one another. This begins to occur at a gas velocity of 120 m/s. At the end of the domain, the intermediate wave is absorbed by the main wave (greatest amplitude). As for the simulation with the steam velocity of 125 m/s, the waves interact with each other. As the highest wave is flowing faster than the intermediate wave, it collapses to form a wave. This absorption takes place earlier than in the case at $v_g = 120\ m/s$. By further increasing the vapor velocity up to 130 m/s, absorption of the intermediate wave by the highest wave is made even earlier than in the case of $v_g = 125\ m/s$. This new wave will then accelerate and grow up to 190 μm. The local Reynolds number is then about 70, which remains approximately in the range of validity of the model. The same pattern is accentuated for a steam velocity of 135 m/s. Indeed, the absorbing wave has a height of 450 μm. The local Reynolds number is then about 1000, which largely exceeds the model's validity range. It should be noted that this simulation is highly unsteady. When the velocity of the vapor is too high, the film has a solitary wave with a strong curvature gradient and a high amplitude. It is implausible to observe this behavior in reality. Indeed, one possible explanation would be that these waves are unstable with respect to 3D perturbations or that drops are torn off at the free surface or that the film takes off from the wall. These three possibilities are actually not taken into account in the simulations of this test case.

4.2.3 Unsteady sheared film with noise forcing

In the [Hammitt et al., 1981] experiment, waves at the free surface of the liquid film on a plate under low-pressure turbine conditions were observed (see paragraph 4.2.1). The experimental estimate of the characteristics of these waves can be summarized as follows: the amplitude of the waves is about 20 % of the average height of the film, the frequency f is in the range [10 - 100] Hz, with a preponderance of 10 Hz and the wave propagation speed c is in the range of 0.01 to 1 m/s. The present validation case aims at comparing these unsteady characteristics with the Stator model expression (57).

In order to recover the natural characteristics of the sheared film, a noise is enforced at the inlet. This noise is constructed with a wide frequency range, each signal having the same amplitude so as not to favor any frequency. The frequency range is chosen between 1 Hz and the analytical cutoff frequency f_c. This corresponds to the frequency beyond which the film remains flat/stable. In other words, frequencies above the cut-off frequency produce disturbances that will be attenuated. This method which was introduced by [Chang et al., 1996], has been used in particular by [Kalliadasis et al., 2011] and [Dietze and Ruyer-Quil, 2013].

By imposing this signal (or noise) (60), the system will then choose the natural frequency of the configuration.

$$\psi(t) = \varepsilon \sum_{f=1}^{f_c} cos(2\pi f t - \phi_f) \tag{60}$$

with the phase ϕ_f generated randomly for each frequency, which lies between 0 and 2π: ε is the constant amplitude of the signal taken at 10^{-2}. The boundary condition at the entrance is thus:

$$\begin{aligned} h(y=0,t) &= h_0(1+\psi(t)) \\ \overline{v}(y=0,t) &= v_0(1+\psi(t)) \end{aligned} \tag{61}$$

where h_0 and v_0 are the height and velocity obtained in the steady case, respectively $h_0 = 130.2\ \mu m$ and $v_0 = 0.0576\ m/s$ (see paragraph 4.2.1) for a given steam velocity. The cutoff frequency f_c, which is the transition value between the stable and unstable perturbations, is obtained with the dispersion relation of the Stator model, resulting from the stability analysis presented in appendix C. For our case, $f_c = 205\ Hz$.

Figure 15 shows the film thickness at time $t = 4\ s$ for a steam velocity of 100 m/s using different meshes.

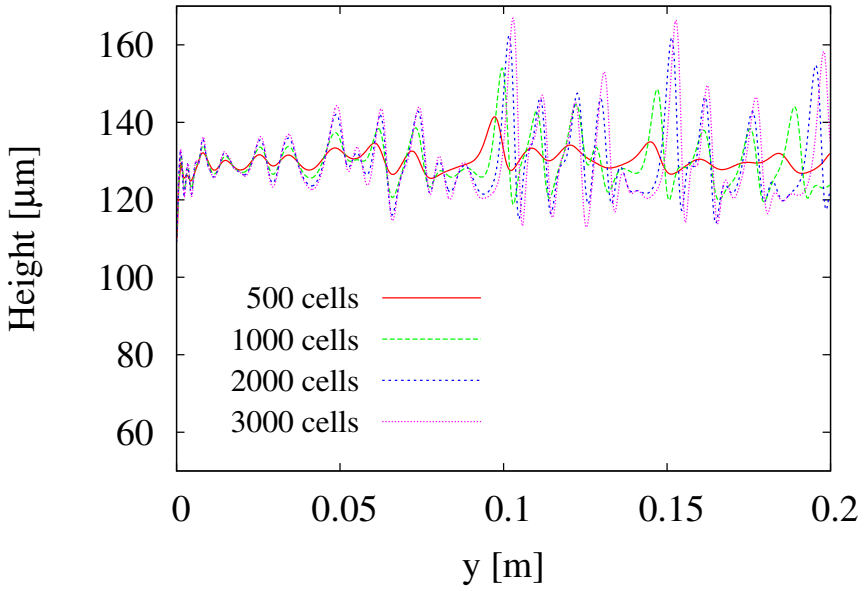

Figure 15: Effect of mesh refinement for a sheared film in low-pressure turbine condition with noise at the inlet boundary. Height in μm for $v_g = 100\ m/s$ at $t = 4\ s$.

A preliminary simulation is performed without any forcing, using a mesh including 3000 cells. In that case, the film remains flat. Figure 16 shows the film height and velocity approximations obtained with 3000 cells.

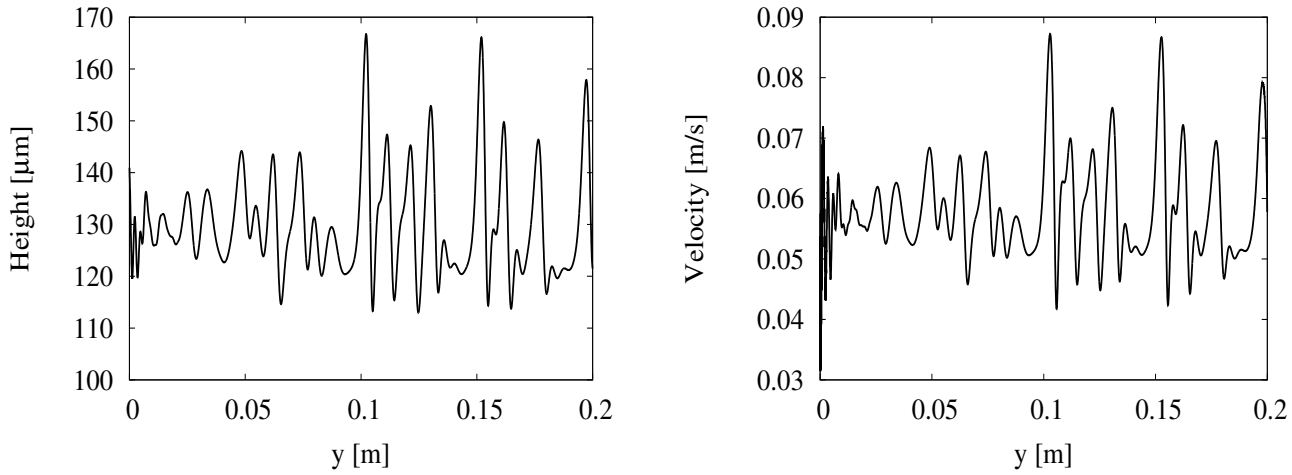

Figure 16: Height (left) and velocity (right) of the film with noise at the entrance and a steam velocity of 100 m/s at $t = 4\ s$ with 3000 cells

The numerical frequencies of the waves at the free surface on figure 16 are extracted with a classical FFT method. These natural frequencies range from 1 Hz to 50 Hz. The frequencies 7 Hz, 10 Hz and 15 Hz are the predominant frequencies. The maximum amplitude of the film, obtained as shown in figure 16, is approximately 20 % of the base height and the wavelength of about 13 mm. To conclude on the validity of the Stator model, more precise experimental data are required. However, the results are encouraging since the results of the Stator model correctly match the estimates of the [Hammitt et al., 1981] experiment detailed in the introduction of this test case.

The impact of the profile factor Γ, introduced in paragraph 2.3 is studied in the case of an unsteady film sheared by steam in a low-pressure turbine condition and with noise at the inlet boundary.

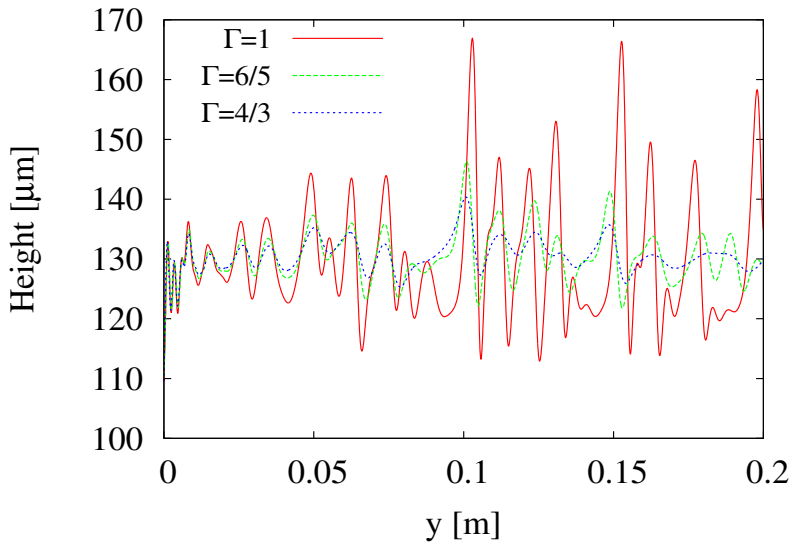

Figure 17: Height of the film for three profile factors (vertical for $\Gamma = 1$, linear for $\Gamma = 4/3$ and semi-parabolic $\Gamma = 6/5$) a steam velocity of 100 m/s for 3000 cells at $t = 4$ s

Figure 17 shows that the profile factor has little influence on the film frequency and the average height value. However, it can be seen that the model with $\Gamma = 4/3$ (linear velocity profile) produces waves with peaks of smaller amplitudes than the model with $\Gamma = 6/5$ (semi- parabolic) and that the model with $\Gamma = 1$ (vertical velocity profile). This conclusion enriches the interpretation of the falling film in non linear-regime test case (see paragraph 4.1.2). In this case, the Stator model with a vertical velocity profile overestimates the peak amplitude compared to the references models of [Ruyer-Quil and Manneville, 2000] and [Lavalle, 2014], which assume a semi-parabolic velocity profile. Ultimately, the type of velocity profile assumed is a preponderant parameter on the amplitude of the waves.

5 Conclusions and discussions

In order to study liquid film in steam turbine, a 2D unsteady model is developed. The model is relatively simple (Shallow-Water type) but stages various physical phenomenon such as the mass transfer, the droplet impact, the rotation and the surface tension. The development of this model is done rigorously by specifying the simplifying assumptions used. It is shown in particular that the momentum due to the droplet impact does not need to be added as an external force. The integration step makes this term appear naturally as long as there is a mass transfer term in the kinematic boundary at the free surface. To fully explain the model, closure laws are proposed in this paper, including an innovative consideration of the velocity involved in the term for the droplets impact.

The model properties analysis underlines that for the closure law $\Gamma = 1$, the model displays a Euler structure for which a wide range of numerical schemes has been proposed in the literature. Besides, the Stator model, as the Shallow-Water equation, is not hyperbolic when the film is located under the wall. This situation corresponds to the case when the gravity has a destabilizing effect and tends to detach the film from the wall. The hyperbolic condition for the Rotor model is found and extends the work of [Tort et al., 2014] to non-constant topography.

Concerning the numerical scheme, the difficulty resides in the surface tension term. This term in integrated formulation models is a third derivative term. Moreover, a von Neumann stability analysis of the numerical

scheme highlights the strong restriction on the time step for fine meshes due to surface tension. This induces a high CPU time.

The simulation aims at judging of the performance of this relative simple model on reference test cases (falling film) and case closer to the final configuration (sheared film). For the falling film in linear regime test case, a linear analysis on the Stator model is performed and shows a different but close theoretical stability threshold compared to the Navier-Stokes equations or reference models for liquid film ([Ruyer-Quil and Manneville, 2000], [Lavalle, 2014] and [Richard et al., 2016]). However, the Stator model represents correctly the threshold feature concerning the presence of waves at the free surface. In a non-linear regime for falling film, the relative simple model with $\Gamma = 1$ displays good results in a view of the complex configuration. It shows the correct free surface form as well as the qualitatively correct wavelength. However it tends to overestimate the amplitude of the waves. As seen in the last test case (noise forcing test case), the non-linear closure law (Γ) impacts in a significant way the amplitude of the waves. Therefore, the use of a Γ other than 1 could lead to more precise results but to the detriment of the structure simplicity that $\Gamma = 1$ offers. Then, if the precision for the falling film case needs to be increased, it might be preferable to switch to more complex models, such as the new model of [Richard et al., 2016] which takes into account the non vertical nature of the velocity profile and has a simple structure (Euler structure). However, to study the full situation of liquid film in steam turbine, the model proposed in this paper in more suitable as it contains more physics.

The most representative experiment which we know of regarding liquid films in steam turbine is the ([Hammitt et al., 1981]) experiment. It measures liquid film heights on a horizontal plate highly sheared by low-pressure steam. The Stator model in comparison of this experiment shows excellent steady results. The unsteady results of the experiment are only estimation of the wave frequency and celerity of the waves but the model stays in the range of these estimations (noise forcing test case). Moreover, the numerical results display the same tendency than the experiment of [Wurz, 1978]: the wavelength increases and the amplitude wave decreases with the increase of the co-current gas velocity. More precise unsteady measurements are needed to fully validate the model. Finally, the mono-forcing test case underlines the hight unsteady and non-linear features which occurs for high shear. It also demonstrates the striking importance to take the surface tension into account and of interpreting results only for local Reynolds number in the validity domain in which has been developed to model.

Acknowledgments
This work were possible thanks to the financial support provided by EDF and ANRT under grant CIFRE 2013/1115 and also thanks to the computational facilities provided by EDF.

A Appendix A: Closure law for the free surface velocity

To obtain information on the velocity at the free surface of the film associated with the mass transfer, a statistical formulation is adopted. Only in the appendix, the water liquid film surrounded by the steam is represented by a statistic two phase model ([Hérard and Hurisse, 2012]). The closure law will verify the physical property of dissipation (or physical entropy increase) for a close domain without external force. We assume that the velocity at the free surface depends on the velocity of both phases. By using the entropy equation of the model, theses restrictions lead to admissible solutions of the free surface velocity.

A.1 The two-phase flow model

The expression of the statistical two-phase flow model is:

$$\begin{cases} \dfrac{\partial \alpha_k}{\partial t} + V_I \dfrac{\partial \alpha_k}{\partial x} = \Phi_k \\ \dfrac{\partial m_k}{\partial t} + \dfrac{\partial m_k U_k}{\partial x} = \gamma_k \\ \dfrac{\partial m_k U_k}{\partial t} + \dfrac{\partial}{\partial x}\left(m_k U_k^2 + \alpha_k \mathcal{P}_k\right) - \mathcal{P}_I \dfrac{\partial \alpha_k}{\partial x} = \mathcal{D}_k + \gamma_k \upsilon_i \end{cases} \tag{62}$$

The model (62) conveys the fact that the statistical presence rate α_k moves at the velocity V_I and depends of a interface transfer term Φ_k, each phase being written k. The mass balance equation with unknown $\boldsymbol{m}_k = \alpha_k \rho_k$ where ρ_k is the density, has a source term γ_k associated with mass transfer. The momentum, $\boldsymbol{m}U$ with U the statistic average velocity is function of the drag $\mathcal{D}_k$, and the "dynamical" mass transfer $\gamma_k \upsilon_i$ with υ_i, the velocity at the free surface. The interface velocity V_I can be estimated using the following strategy. We assume that V_I is a convex combination of phase velocities:

$$V_I = aU_1 + (1-a)U_2 \text{ with } a = f(\underline{W}) \in [0,1] \text{ and } \underline{W} \text{ the vector such that: } \underline{W} = (\alpha_k, \boldsymbol{m}_k, \boldsymbol{m}_k U_k)^T, \tag{63}$$

and also that the interface pressure P_I takes the form:

$$P_I = (a-1)P_1 + aP_2 \tag{64}$$

We recall that:

$$\alpha_1 + \alpha_2 = 1 \text{ with } \alpha_k \in [0,1] \tag{65}$$

We also assume that:

$$\upsilon_i = bU_1 + (1-b)U_2 \text{ with } b \in [0,1] \tag{66}$$

and we know that the interface transfer terms verify:

$$\begin{cases} \mathcal{D}_1 + \mathcal{D}_2 = 0, \\ \Phi_1 + \Phi_2 = 0, \\ \gamma_1 + \gamma_2 = 0 \end{cases} \tag{67}$$

A.2 Governing equation for the total energy

We assume the solutions to be regular. Classical calculations yield:

$$\frac{\partial}{\partial t}\left(\frac{\boldsymbol{m}_k U_k^2}{2}\right) + \frac{\partial}{\partial x}\left(\frac{\boldsymbol{m}_k U_k^3}{2} + \alpha_k \mathcal{P}_k U_k\right) - \alpha_k \mathcal{P}_k \frac{\partial U_k}{\partial x} - U_k \mathcal{P}_I \frac{\partial \alpha_k}{\partial x} = U_k \gamma_k \upsilon_i + U_k \mathcal{D}_k - \frac{U_k^2}{2}\gamma_k \tag{68}$$

With help of first equation in model (62), we obtain:

$$\frac{\partial \rho_k}{\partial t} + \rho_k \frac{\partial U_k}{\partial x} + \frac{\rho_k}{\alpha_k}(U_k - V_I)\frac{\partial \alpha_k}{\partial x} + U_k \frac{\partial \rho_k}{\partial x} - \frac{\gamma_k}{\alpha_k} = -\frac{\rho_k}{\alpha_k}\Phi_k \tag{69}$$

Since each pressure phase only depends on the density, we perform the change of variable $\psi_k'(\rho_k) = \mathcal{P}_k(\rho_k)/\rho_k^2$, we obtain:

$$\frac{\partial \psi_k \boldsymbol{m}_k}{\partial t} + \frac{\partial \psi_k \boldsymbol{m}_k U_k}{\partial x} + \boldsymbol{m}_k \psi_k' \rho_k \frac{\partial U_k}{\partial x} + \rho_k^2 \psi_k'(U_k - V_I)\frac{\partial \alpha_k}{\partial x} = \psi_k \gamma_k + \rho_k \gamma_k \psi_k' - \rho_k^2 \psi_k' \Phi_k \tag{70}$$

Adding up equations (68) and (70), and summing over the phases $k = 1, 2$, we get:

$$\frac{\partial \xi}{\partial t} + \frac{\partial \varphi}{\partial x} + \sum_{k=1}^{2}\left(\rho_k^2 \psi_k'(U_k - V_I) - U_k \mathcal{P}_I\right)\frac{\partial \alpha_k}{\partial x} = \sum_{k=1}^{2}\left(U_k \mathcal{D}_k - \mathcal{P}_k \phi_k + \gamma_k\left(U_k\left(\upsilon_i - \frac{U_k}{2}\right) + \left(\psi_k + \frac{\mathcal{P}_k}{\rho_k}\right)\right)\right) \tag{71}$$

defining:

$$\begin{cases} \xi = \displaystyle\sum_{k=1}^{2}\left(\frac{\boldsymbol{m}_k U_k^2}{2} + \psi_k \boldsymbol{m}_k\right) \\ \varphi = \displaystyle\sum_{k=1}^{2}\left(\frac{\boldsymbol{m}_k U_k^3}{2} + \alpha_k \mathcal{P}_k U_k + \alpha_k \rho_k \psi_k U_k\right) \end{cases} \tag{72}$$

or:

$$\frac{\partial \xi}{\partial t} + \frac{\partial \varphi}{\partial x} = \sum_{k=1}^{2}\left(U_k \mathcal{D}_k - \mathcal{P}_k \phi_k + \gamma_k\left(U_k\left(\upsilon_i - \frac{U_k}{2}\right) + \left(\psi_k + \frac{\mathcal{P}_k}{\rho_k}\right)\right)\right) \tag{73}$$

since:

$$\sum_{k=1}^{2}\left(\rho_k^2 \psi_k'(U_k - V_I) - U_k \mathcal{P}_I\right)\frac{\partial \alpha_k}{\partial x} = 0 \tag{74}$$

due to the specific choice of V_I and P_I (see equations (63) and (64))

A.3 Admissible forms of source terms

Since the energy ξ of the two-phase model (62) must decrease in a close domain without any external forces the source term of the equation (71) must be negative. Three distinct phenomena (mass transfer, drag and pressure relaxation) are functions of independent arguments α_i, U_1, $U_1 - U_2$, P_1, $P_1 - P_2$. Therefore, the model (62) is dissipative if and only if the transfer terms, γ_k and ϕ_k dissipate, as well as the term $\mathcal{D}_k$. So that we must enforce:

$$\begin{cases} \mathcal{D}_1(U_1 - U_2) \leq 0, \\ \Phi_1(P_2 - P_1) \leq 0, \\ \gamma_1 \left(\left(\psi_1 + \dfrac{\mathcal{P}_1}{\rho_1} \right) - \left(\psi_2 + \dfrac{\mathcal{P}_2}{\rho_2} \right) + \left(b - \dfrac{1}{2} \right) (U_1 - U_2)^2 \right) \leq 0 \end{cases} \tag{75}$$

Standard forms for the drag $\mathcal{D}_1$ and the pressure relaxation term, Φ_1, which are classically used in the literature:

$$\begin{cases} \mathcal{D}_1 = K_D^2 (U_2 - U_1), \\ \Phi_1 = K_\Phi^2 (P_1 - P_2) \end{cases} \tag{76}$$

with K_D^2 and K_Φ^2 positive constants, comply with constraints (75).

If we turn to the mass transfer term, two closure laws are admissible. The classical approach consists in assuming that the dissipation due to the mass transfer only involves thermodynamic quantities. This implies:

$$\begin{cases} \upsilon_i = \dfrac{1}{2} (U_1 + U_2), \\ \gamma_1 \left(\left(\psi_1 + \dfrac{\mathcal{P}_1}{\rho_1} \right) - \left(\psi_2 + \dfrac{\mathcal{P}_2}{\rho_2} \right) \right) \leq 0 \end{cases} \tag{77}$$

In a second alternative approach, one might consider that the dissipation due to mass transfer comes from both the thermodynamic and the relative velocity between the two phases; in that case, admissible closure laws would be:

$$\begin{cases} \upsilon_i = b U_1 + (1 - b) U_2 \\ \gamma_1 \left(\left(\psi_1 + \dfrac{\mathcal{P}_1}{\rho_1} \right) - \left(\psi_2 + \dfrac{\mathcal{P}_2}{\rho_2} \right) + \left(b - \dfrac{1}{2} \right) (U_1 - U_2)^2 \right) \leq 0 \end{cases} \tag{78}$$

In this paper, we will restrict to the first closure (77). The velocities at the free surface have the expressions:

$$\begin{cases} u_{|_\eta} = \dfrac{(U_1 + U_2)}{2} \\ v_{|_\eta} = \dfrac{(V_1 + V_2)}{2} \end{cases} \tag{79}$$

It should be noted that the result is still valid in a non-barotropic framework [Coquel et al., 2002], focusing on two-phase flows also in the "multi-field" context [Hérard, 2016]. Note that the function $(\psi_k + \mathcal{P}_k/\rho_k)(\rho_k)$ is the specific enthalpy of the phase k, traditionally noted h_k and ψ_k is the internal energy of the phase k.

B Numerical stability analysis including the surface tension

In this appendix, we will check that, the convection and the surface tension impose a restriction on the time step for the model without rotation. For that purpose, we perform a von Neumann stability analysis. The analysis is achieved for the Stator model 1D with $\Gamma = 1$ using a forward Euler temporal scheme, Rusanov flux scheme for convective fluxes and a centered scheme for the surface tension. First, a linearization of the continuous equations around a equilibrium solution is performed. Then, perturbations are introduced in a Fourier series form. Eventually, we seek conditions so that the error amplification would be smaller than 1.

We start with the Stator 1D model with $\Gamma = 1$:

$$\begin{cases} \dfrac{\partial h}{\partial t} + \dfrac{\partial q}{\partial y} = 0 \\ \dfrac{\partial q}{\partial t} + \dfrac{\partial}{\partial y} \left(\dfrac{q^2}{h} + \dfrac{g \cos\theta h^2}{2} \right) = \dfrac{\sigma}{\rho} h \dfrac{\partial^3 h}{\partial y^3} \end{cases} \tag{80}$$

still setting $q = h\overline{v}$; σ and ρ are none zero positive constants.

By linearizing around an equilibrium state (h_0, q_0) such that:

$$\begin{cases} h = h_0 + h' \\ q = q_0 + q' \end{cases} \tag{81}$$

we find the following perturbed system:

$$\frac{\partial \underline{W}'}{\partial t} + \underline{\underline{\mathcal{C}}} \frac{\partial \underline{W}'}{\partial y} - \underline{\underline{\mathcal{D}_\sigma}} \frac{\partial^3 \underline{W}'}{\partial y^3} = 0 \tag{82}$$

with:

$$\underline{W} = \begin{pmatrix} h' \\ q' \end{pmatrix}; \qquad \underline{\underline{\mathcal{C}}} = \begin{pmatrix} 0 & 1 \\ g\cos\theta h_0 - \overline{v}_0^2 & 2\overline{v}_0 \end{pmatrix} \qquad \text{and} \qquad \underline{\underline{\mathcal{D}_\sigma}} = \begin{pmatrix} 0 & 0 \\ \dfrac{\sigma}{\rho} h_0 & 0 \end{pmatrix} \tag{83}$$

We apply now to the perturbed equations the forward Euler scheme, the explicit Rusanov flux scheme and the centered scheme for the surface tension:

$$\begin{aligned} \frac{\underline{W}_j^{'n+1} - \underline{W}_j^{'n}}{\Delta t} + \frac{1}{2\Delta y}\left(\underline{\underline{\mathcal{C}}}\left(\underline{W}_{j+1}^{'n} - \underline{W}_{j-1}^{'n}\right) - \rho_s \left(\underline{\underline{\mathcal{C}}}\right) \underline{\underline{\mathcal{I}_d}} \left(\underline{W}_{j+1}^{'n} - 2\underline{W}_j^{'n} + \underline{W}_{j-1}^{'n}\right)\right) = \\ \frac{\underline{\underline{\mathcal{D}_\sigma}}}{2\Delta y}\left(\underline{W}_{j+2}^{'n} - 2\underline{W}_{j+1}^{'n} + 2\underline{W}_{j-1}^{'n} - \underline{W}_{j-2}^{'n}\right) \end{aligned} \tag{84}$$

Multiplying the expression (84) by $e^{ij\omega}$, with i, the imaginary unit and summing over cells $j \in \mathbb{N}$, and noting $\underline{\overset{\circ}{W}}'$ the following Fourier transform, we have:

$$\underline{\overset{\circ}{W}}' = \sum_{k\in\mathbb{Z}} e^{ik\omega} \underline{W}'_k \tag{85}$$

the discrete form of equation (84) becomes :

$$\frac{d\underline{\overset{\circ}{W}}'}{dt} + \frac{\underline{\overset{\circ}{W}}'}{2\Delta y}\left(\underline{\underline{\mathcal{C}}}\left(e^{-i\omega} - e^{i\omega}\right) - \rho_s \left(\underline{\underline{\mathcal{C}}}\right) \underline{\underline{\mathcal{I}_d}} \left(e^{-i\omega} - 2 + e^{i\omega}\right)\right) = \frac{\underline{\underline{\mathcal{D}_\sigma}}}{2\Delta y}\left(e^{-2i\omega} - 2e^{-i\omega} + 2e^{i\omega} - e^{2i\omega}\right) \underline{\overset{\circ}{W}}' \tag{86}$$

We reorganize the expression (86) and note :

$$\psi = \frac{2}{\Delta y} \sin\left(\frac{\omega}{2}\right) \tag{87}$$

Thus we get:

$$\frac{d\underline{\overset{\circ}{W}}'}{dt} = i\psi \underline{\underline{\mathcal{A}}}(\psi, \Delta y) \underline{\overset{\circ}{W}}' \tag{88}$$

noting:

$$\underline{\underline{\mathcal{A}}}(\psi, \Delta y) = \sqrt{1 - \frac{(\psi\Delta y)^2}{4}} (\underline{\underline{\mathcal{C}}} + \psi^2 \underline{\underline{\mathcal{D}_\sigma}}) + i \frac{\rho_s \left(\underline{\underline{\mathcal{C}}}\right) \underline{\underline{\mathcal{I}_d}}}{2} \Delta y \psi \tag{89}$$

By applying the numerical temporal forward Euler scheme, we have:

$$\underline{\overset{\circ}{W}}'^{n+1} = \left(\underline{\underline{\mathcal{I}_d}} + i\psi\Delta t \underline{\underline{\mathcal{A}}}(\psi, \Delta y)\right) \underline{\overset{\circ}{W}}'^{n} \tag{90}$$

Hence, the scheme is stable if:

$$|\underline{\overset{\circ}{W}}'^{n+1}| \leq |\underline{\overset{\circ}{W}}'^{n}| \tag{91}$$

If λ denotes any eigenvalue of matrix $\underline{\underline{\mathcal{A}}}$, λ:

$$\lambda = R(\psi, \Delta y) + iI(\psi, \Delta y) \tag{92}$$

Then, by choosing an eigenvector basis, the condition (91) becomes:

$$\begin{cases} |1 + i\psi\Delta t(R_+ + iI_+)|^2 \leq 1 \\ |1 + i\psi\Delta t(R_- + iI_-)|^2 \leq 1 \end{cases} \tag{93}$$

equivalently:

$$\begin{cases} \Delta t \leq \dfrac{2\psi I_+}{\psi^2(I_+^2 + R_+^2)} \\ \Delta t \leq \dfrac{2\psi I_-}{\psi^2(I_-^2 + R_-^2)} \end{cases} \tag{94}$$

The eigenvalues $\lambda_\pm$ of matrix $\underline{\underline{\mathcal{A}}}(\psi, \Delta y)$ defined in equation (89) are:

$$\lambda_\pm = Z\left(\overline{v}_0 \pm \sqrt{c_0^2 + \psi^2\overline{\sigma}}\right) + \frac{1}{2}\rho_s\left(\underline{\underline{\mathcal{C}}}\right)\Delta y i\psi \tag{95}$$

with:

$$\begin{cases} Z = \sqrt{1 - \dfrac{(\psi\Delta y)^2}{4}} \\ \overline{\sigma} = \dfrac{\sigma h_0}{\rho} \\ c_0^2 = g\cos\theta h_0 \end{cases} \tag{96}$$

If we introduce:

$$s = \frac{\delta y^2}{4}\psi^2 = \frac{\sin^2\omega}{2} \tag{97}$$

the explicit stability condition (94) will be:

$$\left(s\frac{\Delta t}{\Delta y}\rho_s\left(\underline{\underline{\mathcal{C}}}\right) + (1-s)\frac{\Delta t}{\Delta y}\rho_s\left(\underline{\underline{\mathcal{C}}}\right)\left(\overline{v}_0 \pm \sqrt{c_0^2 + \frac{4\overline{\sigma}}{\Delta y^2}s}\right)^2\right) \leq 1 \tag{98}$$

Eventually, as $s \in [0, 1]$, a sufficient condition to comply with inequality (98) is :

$$\max\left(\frac{\Delta t}{\Delta y}\rho_s\left(\underline{\underline{\mathcal{C}}}\right), \frac{\Delta t}{\Delta y}\rho_s\left(\underline{\underline{\mathcal{C}}}\right)\left(|\overline{v}_0| + \sqrt{c_0^2 + \frac{4\overline{\sigma}}{\Delta y^2}}\right)^2\right) \leq 1 \tag{99}$$

We then find the stability condition for the model (80), discretized in Forward Euler scheme with the Rusanov flux and with a centered scheme for the dispersion term. For coarse meshes, the time step is ruled by convection, whereas for fine meshes, the time step is driven by surface tension effects.

C Linear stability analysis

In this appendix, linear stability analyses on the Stator model for falling film on inclined planes are investigated. It is showed that for two different linearizations, the same stability threshold is found. The analyses are performed without doing an asymptotic expansion on the wave velocity c (or on the angular velocity ω) as did [Ruyer-Quil and Manneville, 2000], [Luchini and Charru, 2010], [Lavalle, 2014] with their own model but by doing a asymptotic expansion in respect to the wave-number k. The principle of the analysis is to construct the perturbed linear equations around a stationary state called base-state, indexed by a 0. Then, by giving a form of perturbation, we find a relation between the angular velocity (or the celerity of the waves) and the wave number, called the dispersion relation. A change of variable for the dispersion relation leads to a bi-quadratic function which can be exactly solved, then approximated under the long wavelengths assumption. This leads to the bifurcation threshold in function of the Reynolds number of the base-state flow Re, or in a equivalent manner in function of the Froude number of the base-state flow Fr. This study also establishes the neutral stability effect of the surface tension for long wavelengths.

C.1 Governing equations

In the model developed in this paper, the continuity equation and the $y-$momentum equation with $\Gamma = 1$, the gravity source term, the surface tension and the friction at the wall (assuming a semi-parabolic velocity profile and no shear-stress at the free surface) represents a falling film on a inclined plane, as is showed on figure 18.

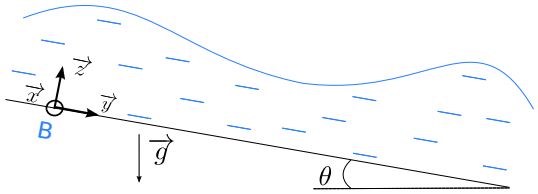

Figure 18: Scheme of a falling film on a inclined plane

The expression of the model is recalled below:

$$\begin{cases} \dfrac{\partial h}{\partial t} + \dfrac{\partial h\overline{v}}{\partial y} = 0 \\ \dfrac{\partial h\overline{v}}{\partial t} + \dfrac{\partial}{\partial y}\left(h\overline{v}^2 + \dfrac{g\cos\theta h^2}{2}\right) = gh\sin\theta - \dfrac{3\nu\overline{v}}{h} + \dfrac{\sigma}{\rho}h\dfrac{\partial^3 h}{\partial y^3} \end{cases} \tag{100}$$

We define the following non-dimensional numbers using the base-state (solution for an equilibrium flow) h_0 and v_0 (with $q_0 = h_0 v_0$):

$$\begin{cases} Re = \dfrac{h_0 v_0}{\nu} \\ Fr = \dfrac{v_0}{\sqrt{g h_0}} \\ We = \dfrac{\rho h_0 v_0^2}{\sigma} \end{cases} \tag{101}$$

At the equilibrium, the gravity forces compensate the friction at the wall leading to a relation between the base-state Reynolds number and the base-state Froude number:

$$\frac{\sin\theta}{Fr^2} = \frac{3}{Re} \tag{102}$$

C.2 Resolution with the variables h and $\overline{v}$

We consider infinitesimal perturbations h', $\overline{v}'$ around the equilibrium state h_0, $\overline{v}_0$:

$$\begin{cases} h = h_0 + h' \ \text{ with } \ h' \ll h_0 \\ \overline{v} = \overline{v}_0 + \overline{v}' \ \text{ avec } \ v' \ll v_0 \end{cases} \tag{103}$$

By replacing the expressions (103) in the model (100), the new variables become the perturbed height, h' and velocity, $\overline{v}'$. To deal with the friction term, a Taylor-expansion is made for small perturbations such that $(1 + h'/h_0)^{-1} \simeq 1 - h'/h_0 + \mathcal{O}(h'^2)$. Then, the linearization consists in neglecting unknowns above power of two which gives:

$$\begin{cases} \dfrac{\partial h'}{\partial t} + \overline{v}_0\dfrac{\partial h'}{\partial y} + h_0\dfrac{\partial \overline{v}'}{\partial y} = 0 \\ \dfrac{\partial \overline{v}'}{\partial t} + \overline{v}_0\dfrac{\partial \overline{v}'}{\partial y} + g\cos\theta\dfrac{\partial h'}{\partial y} - g\sin\theta\dfrac{h'}{h_0} + \dfrac{3\nu\overline{v}'}{{h_0}^2} - \dfrac{3\nu\overline{v}_0 h'}{{h_0}^3} - \dfrac{\sigma}{\rho}\dfrac{\partial^3 h'}{\partial y^3} = 0 \end{cases} \tag{104}$$

The perturbations are sought in the form:

$$\underline{\Phi} = \underline{\hat{\Phi}}\exp^{ik(y-ct)} \tag{105}$$

with $\underline{\Phi} = (h', \overline{v}')^T$. By replacing the form of the perturbations expression (105) in the linearized model (104), one can obtain the relation dispersion that links the celerity of the complex waves c to the real wave number k:

$$c^2 - 2\overline{v}_0 c + {\overline{v}_0}^2 + (c - \overline{v}_0)\,\frac{3\nu}{h_0^2}\frac{i}{k} - h_0\left(g\cos\theta + \frac{\sigma}{\rho}k^2\right) - \frac{i}{k}\left(g\sin\theta + \frac{3\nu\overline{v}_0}{h_0^2}\right) = 0 \tag{106}$$

To solve this dispersion relation, this one is splitted into its real part and imaginary part. Moreover, the change of variable $\zeta = (\overline{v}_0 - c_r)/\overline{v}_0$ has the advantage to transform the dispersion relation into a system of a linear function and a bi-quadratic function. The system expressed in non-dimensional numbers defined in expression (101) is:

$$\begin{cases} c_i = -\dfrac{\overline{v}_0}{2(h_0 k)}\left(\dfrac{3}{Re} + \left(\dfrac{3}{Re} + \dfrac{\sin\theta}{Fr^2}\right)\dfrac{1}{\zeta}\right) \\ \zeta^4 - \zeta^2\left(\dfrac{\cos\theta}{Fr^2} + \dfrac{(h_0 k)^2}{We} - \dfrac{9}{4Re^2(h_0 k)^2}\right) - \dfrac{1}{4Fr^4}\left(\sin\theta + \dfrac{3Fr^2}{Re}\right)^2\left(\dfrac{1}{h_0 k}\right)^2 = 0 \end{cases} \tag{107}$$

The liquid film becomes unstable when the perturbations are amplified that is to say when the imaginary part of the celerity wave, c_i is positive, so when:

$$\frac{3}{Re} + \left(\frac{3}{Re} + \frac{\sin\theta}{Fr^2}\right)\frac{1}{\zeta} < 0 \tag{108}$$

To determine the instability threshold as a function of the variables of the base-state flow, ζ has to be explicited. The bi-quadratic equation, defined in the system (107), is reduced to a polynomial of order two by the change of variable $\zeta^2 = \hat{\zeta}$. The discriminant of this new function, $\hat{\zeta}$, is positive and then admits two distinct real roots, $\hat{\zeta}_+$ and $\hat{\zeta}_-$. The product of these roots is negative, therefore the two roots are of opposite signs. As $\hat{\zeta}$ is the square of ζ, only the positive root of $\hat{\zeta}$, denoted $\hat{\zeta}_+$ is admissible:

$$\zeta^2 = \hat{\zeta}_+ = \frac{-b + \sqrt{\Delta}}{2} \tag{109}$$

with:

$$b = \frac{9}{4Re^2(h_0 k)^2} - \frac{\cos\theta}{Fr^2} - \frac{(h_0 k)^2}{We} \tag{110}$$

and:

$$\Delta = b^2 + \frac{1}{Fr^4}\left(\sin\theta + \frac{3Fr^2}{Re}\right)^2\left(\frac{1}{h_0 k}\right)^2 \tag{111}$$

Moreover, the relation (108) implies that for ζ positive, the liquid film is always stable. We are interested in the negative root of ζ, denoted by ζ_-:

$$\zeta_- = -\zeta_+ = -\sqrt{\hat{\zeta}_+} \tag{112}$$

The stability condition (108), squared to simplify the calculations, becomes:

$$\frac{9}{Re^2}\hat{\zeta}_+ - \left(\frac{3}{Re} + \frac{\sin\theta}{Fr^2}\right)^2 < 0 \tag{113}$$

We put $X = h_0 k$ and we express the stability condition defined in equation (113) as a function of X:

$$\frac{9}{2Re^2}\left(\frac{\cos\theta X^2}{Fr^2} + \frac{X^4}{We} - \frac{9}{4Re^2} + \sqrt{X^4\Delta}\right) - X^2\left(\frac{3}{Re} + \frac{\sin\theta}{Fr^2}\right)^2 < 0 \tag{114}$$

Under the approximation of long wavelengths ($\lambda \to\infty$ or $X \to 0^+$) and using an expansion to the order 2 with respect to X, the relation (114) determines that the film is unstable for $Re > Re_{cr}$. This condition can also be expressed as a function of the Froude number using the equilibrium relation (102):

$$\begin{cases} Re_{cr} = \dfrac{3\cot\theta}{4}, \\ Fr_{cr} = \dfrac{\sqrt{\cos\theta}}{2} \end{cases} \tag{115}$$

Moreover, since the stability criterion does not depend on the effect of the surface tension, it has a neutral effect for long wavelengths.

C.3 Resolution with the variables h and q

The advantage of considering the set of variables h and q is that the continuity equation on the linearized perturbations remains unchanged with respect to the model (100). Let's consider an infinitesimal perturbation on height and flow such that $h = h_0 + h'$ and $q = q_0 + q'$.

$$\begin{cases} \dfrac{\partial h'}{\partial t} + \dfrac{\partial q'}{\partial y} = 0 \\ \dfrac{\partial q'}{\partial t} + 2\overline{v}_0 \dfrac{\partial q'}{\partial y} - {\overline{v}_0}^2 \dfrac{\partial h'}{\partial y} + g\cos\theta h_0 \dfrac{\partial h'}{\partial y} - g\sin\theta h' + \dfrac{3\nu q'}{{h_0}^2} - \dfrac{6\nu q_0 h'}{{h_0}^3} - \dfrac{\sigma h_0}{\rho}\dfrac{\partial^3 h'}{\partial y^3} = 0 \end{cases} \tag{116}$$

The perturbations are sought in the form:

$$\underline{\Phi} = \hat{\underline{\Phi}} \exp^{ik(y-ct)} \tag{117}$$

with $\underline{\Phi} = (h', q')^T$. By replacing the expression (117) in the linearized model (116), the non-trivial solution is obtained by solving the following dispersion relation:

$$c^2 - 2\overline{v}_0 c + {\overline{v}_0}^2 - h_0\left(g\cos\theta + \frac{\sigma}{\rho}k^2\right) + \frac{i}{k}\left(\frac{3\nu}{h_0^2}(c - 2\overline{v}_0) - g\sin\theta\right) = 0 \tag{118}$$

The change of variable $\zeta = (\overline{v}_0 - c_r)/\overline{v}_0$ is used to solve the dispersion relation more easily. By doing an expansion on the small number of waves, we obtain the unstable domain in terms of Reynolds number ($Re > Re_{cr}$) or Froude number ($Fr > Fr_{cr}$) using the equilibrium relation (102):

$$\begin{cases} Re_{cr} = \dfrac{3\cot\theta}{4}, \\ Fr_{cr} = \dfrac{\sqrt{\cos\theta}}{2} \end{cases} \tag{119}$$

We notice then that the instability threshold is the same as for the linearization on the variable h and $\overline{v}$. As for the linearization with h and $\overline{v}$, the surface tension does not appear in the expression on the system stability threshold (119). Then it has a neutral effect for long wavelengths.

References

[Baumann, 1912] Baumann, K. (1912). Recent developments in steam turbine practice. *Journal of the Institution of Electrical Engineers*, 48(213):768–842.

[Blondel, 2014] Blondel, F. (2014). *Couplages instationnaires de la vapeur humide dans les écoulements de turbines à vapeur*. PhD thesis, Ecole Centrale de Lyon, https://tel.archives-ouvertes.fr/tel-00985725.

[Chang et al., 1996] Chang, H.-C., Demekhin, E. A., and Kalaidin, E. (1996). Simulation of noise-driven wave dynamics on a falling film. *AIChE journal*, 42(6):1553–1568.

[Coquel et al., 2002] Coquel, F., Gallouët, T., Hérard, J.-M., and Seguin, N. (2002). Closure laws for a two-fluid two-pressure model. *Comptes Rendus Mathematique*, 334(10):927–932.

[Delestre, 2010] Delestre, O. (2010). *Simulation du ruissellement d'eau de pluie sur des surfaces agricoles*. PhD thesis, Université d'Orléans, https://tel.archives-ouvertes.fr/tel-00531377.

[Dietze and Ruyer-Quil, 2013] Dietze, G. F. and Ruyer-Quil, C. (2013). Wavy liquid films in interaction with a confined laminar gas flow. *Journal of Fluid Mechanics*, 722:348–393.

[Fendler, 2012] Fendler, Y. (2012). *Analyse des phénomènes liés à la présence de la phase liquide dans les turbines à vapeur et élaboration de modèles méridiens pour en prédire les effets*. PhD thesis, Ecole Centrale de Lyon, https://tel.archives-ouvertes.fr/tel-00818336.

[Foucart, 1999] Foucart, H. (1999). *Modélisation tridimensionnelle des films liquides pariétaux dans les moteurs à combustion interne*. PhD thesis, Université de Rouen.

[Gyarmathy, 1962] Gyarmathy, G. (1962). *Grundlagen einer theorie der nassdampfturbine*. PhD thesis, Diss. Techn. Wiss. ETH Zürich, http://e-collection.library.ethz.ch/eserv/eth:31854/eth-31854-02.pdf.

[Hammitt et al., 1981] Hammitt, F. G. et al. (1981). Liquid film and droplet stability consideration as applied to wet steam flow. *Forschung im Ingenieurwesen A*, 47(1):1–14.

[Hérard, 2016] Hérard, J.-M. (2016). A class of compressible multiphase flow models. *Comptes Rendus Mathématique*, 354(9):954–959.

[Hérard and Hurisse, 2012] Hérard, J.-M. and Hurisse, O. (2012). A fractional step method to compute a class of compressible gas–liquid flows. *Computers & Fluids*, 55:57–69.

[Iapws,] Iapws. web site: http://www.iapws.org/.

[Ihnatowicz et al., 1979] Ihnatowicz, E., Gumkowski, S., and Mikielewicz, J. (1979). Experimental study of evaporation and breakdown of thin liquid films driven by shear stresses. *Journal of Heat Transfer*, 101(4):712–717.

[Kalliadasis et al., 2011] Kalliadasis, S., Ruyer-Quil, C., Scheid, B., and Velarde, M. G. (2011). *Falling liquid films*, volume 176. Springer Science & Business Media.

[Kirillov and Yablonik, 1970] Kirillov and Yablonik (1970). *Fundamentals of the theory of turbines operating on wet steam*. National Aeronautics and Space Administration TT F-611.

[Laali, 1991] Laali, A. (1991). A new approach for assessment of the wetness losses in steam turbines. In *Turbomachinery: latest developments in a changing scene*.

[Lavalle, 2014] Lavalle, G. (2014). *Integral modeling of liquid films sheared by a gas flow*. PhD thesis, ISAE-Institut Supérieur de l'Aéronautique et de l'Espace, https://tel.archives-ouvertes.fr/tel-01139899.

[Liu and Gollub, 1994] Liu, J. and Gollub, J. P. (1994). Solitary wave dynamics of film flows. *Physics of Fluids*, 6(5):1702–1712.

[Luchini and Charru, 2010] Luchini, P. and Charru, F. (2010). Consistent section-averaged equations of quasi-one-dimensional laminar flow. *Journal of Fluid Mechanics*, 656:337–341.

[Malamatenios et al., 1994] Malamatenios, C., Giannakoglou, K., and Papailiou, K. (1994). A coupled two-phase shear layer/liquid film calculation method. formulation of the physical problem and solution algorithm. *International journal of multiphase flow*, 20(3):593–612.

[Moore and Sculpher, 1969] Moore, M. and Sculpher, P. (1969). Paper 19: Conditions producing concentrated erosion in large steam turbines. In *Proceedings of the Institution of Mechanical Engineers, Conference Proceedings*, volume 184, pages 45–56. SAGE Publications.

[Moore and Sieverding, 1976] Moore, M. J. and Sieverding, C. (1976). Two-phase steam flow in turbines and separators: theory, instrumentation, engineering.

[Noble and Vila, 2014] Noble, P. and Vila, J.-P. (2014). Stability theory for difference approximations of euler–korteweg equations and application to thin film flows. *SIAM Journal on Numerical Analysis*, 52(6):2770–2791.

[Richard and Gavrilyuk, 2012] Richard, G. and Gavrilyuk, S. (2012). A new model of roll waves: comparison with brock's experiments. *Journal of Fluid Mechanics*, 698:374–405.

[Richard et al., 2016] Richard, G., Ruyer-Quil, C., and Vila, J. (2016). A three-equation model for thin films down an inclined plane. *Journal of Fluid Mechanics*, 804:162–200.

[Ruyer-Quil and Manneville, 1998] Ruyer-Quil, C. and Manneville, P. (1998). Modeling film flows down inclined planes. *The European Physical Journal B-Condensed Matter and Complex Systems*, 6(2):277–292.

[Ruyer-Quil and Manneville, 2000] Ruyer-Quil, C. and Manneville, P. (2000). Improved modeling of flows down inclined planes. *The European Physical Journal B-Condensed Matter and Complex Systems*, 15(2):357–369.

[Schuster et al., 2014] Schuster, S., Benra, F.-K., Dohmen, H. J., König, S., and Martens, U. (2014). Sensitivity analysis of condensation model constants on calculated liquid film motion in radial turbines. In *Turbo Expo 2014*. American Society of Mechanical Engineers, http://proceedings.asmedigitalcollection.asme.org/proceeding.aspx?articleid=1907367.

[Simon, 2017] Simon, A. (2017). *Modélisation et simulation des films liquides dans les turbines à vapeur*. PhD thesis, Ecole Centrale Lyon, https://tel.archives-ouvertes.fr/tel-01490442.

[Simon et al., 2016] Simon, A., Marcelet, M., Hérard, J.-M., Dorey, J.-M., and Lance, M. (2016). A model for liquid films in steam turbines and preliminary validations. In *ASME Turbo Expo 2016: Turbomachinery Technical Conference and Exposition*, pages Paper No. GT2016–56148, pp. V008T26A007. American Society of Mechanical Engineers, doi:10.1115/GT2016-56148.

[Spedding and Hand, 1997] Spedding, P. and Hand, N. (1997). Prediction in stratified gas-liquid co-current flow in horizontal pipelines. *International journal of heat and mass transfer*, 40(8):1923–1935.

[Stanciu et al.,] Stanciu, M., Marcelet, M., and Dorey, J.-M. Numerical investigation of condenser pressure effect on last stage operation of low pressure wet steam turbines. In *Turbo Expo 2013*. American Society of Mechanical Engineers, doi:10.1115/GT2013-94070.

[Stanton and Rutland, 1998] Stanton, D. W. and Rutland, C. J. (1998). Multi-dimensional modeling of thin liquid films and spray-wall interactions resulting from impinging sprays. *International Journal of Heat and Mass Transfer*, 41(20):3037–3054.

[Tort et al., 2014] Tort, M., Dubos, T., Bouchut, F., and Zeitlin, V. (2014). Consistent shallow-water equations on the rotating sphere with complete coriolis force and topography. *Journal of Fluid Mechanics*, 748:789–821.

[Wehausen and Laitone, 1960] Wehausen, J. V. and Laitone, E. V. (1960). *Surface waves*. Springer.

[White, 1992] White, A. J. (1992). *Condensation in steam turbine cascades*. PhD thesis, Uni. of Cambridge.

[Williams and Young, 2007] Williams, J. and Young, J. B. (2007). Movement of deposited water on turbomachinery rotor blade surfaces. *Journal of turbomachinery*, 129(2):394–403.

[Wurz, 1978] Wurz, D. (1978). Subsonic and supersonic gas-liquid film flows. *AlAA 11TH FLUID AND PLASMA DYNAMICS CONFERENCE, https://doi.org/10.2514/6.1978-1130*.

[Zaichik et al., 2010] Zaichik, L., Drobyshevsky, N., Filippov, A., Mukin, R., and Strizhov, V. (2010). A diffusion-inertia model for predicting dispersion and deposition of low-inertia particles in turbulent flows. *International Journal of Heat and Mass Transfer*, 53(1):154–162.

[Zaichik et al., 1995] Zaichik, L., Nigmatulin, B., and Pershukov, V. (1995). Modelling of dynamics of aerosols in near-wall turbulent flows and particle deposition in pipes. In *Proceedings of the 2nd International Conference on Multiphase Flow*, volume 4, pages 9–16.